Genome-scale clustered regularly interspaced short palindromic repeats screen identifies nucleotide metabolism as an actionable therapeutic vulnerability in diffuse large B-cell lymphoma

Nicholas Davies,[1*] Tegan Francis,[1*] Ceri Oldreive,[1] Maria Azam,[1] Jordan Wilson,[1] Philip J. Byrd,[1] Megan Burley,[1] Archana Sharma-Oates,[2] Peter Keane,[1] Sael Alatawi,[1,3] Martin R. Higgs,[1] Zbigniew Rudzki,[4] Maha Ibrahim,[1,5] Tracey Perry,[1] Angelo Agathanggelou,[1] Anne-Marie Hewitt,[1] Edward Smith,[1] Constanze Bonifer,[1] Mark O'Connor,[6] Josep V. Forment,[6] Paul G. Murray,[7] Eanna Fennell,[7] Gemma Kelly,[8] Catherine Chang,[8] Grant S. Stewart,[1] Tatjana Stankovic,[1] Marwan Kwok[1,9] and Alexander Malcolm Taylor[1]

[1]Institute of Cancer and Genomic Sciences, University of Birmingham, Birmingham, UK; [2]School of Biosciences, University of Birmingham, Birmingham, UK; [3]Department of Medical Laboratory Technology, Faculty of Applied Medical Sciences, University of Tabuk, Tabuk, Saudi Arabia; [4]Department of Histopathology, University Hospitals Birmingham NHS Foundation Trust, Birmingham, UK; [5]South Egypt Cancer Institute, Assiut University, Assiut, Egypt; [6]Bioscience Oncology R&D, AstraZeneca, Cambridge, UK; [7]School of Medicine, Bernal Institute, Health Research Institute & LDCRC, University of Limerick, Limerick, Ireland; [8]Blood Cells and Blood Cancer Division, The Walter and Eliza Hall Institute of Medical Research, Melbourne, Victoria, Australia and [9]Center for Clinical Hematology, Queen Elizabeth Hospital Birmingham, Birmingham, UK

*ND and TF contributed equally as first authors.

Correspondence: T. Stankovic
t.stankovic@bham.ac.uk

A.M. Taylor
a.m.r.taylor@bham.ac.uk

M. Kwok
m.kwok@bham.ac.uk

Received: October 4, 2023.
Accepted: May 24, 2024.
Early view: June 6, 2024.

https://doi.org/10.3324/haematol.2023.284404

Abstract

Diffuse large B-cell lymphoma (DLBCL) is the most common malignancy that develops in patients with ataxia-telangiectasia, a cancer-predisposing inherited syndrome characterized by inactivating germline *ATM* mutations. *ATM* is also frequently mutated in sporadic DLBCL. To investigate lymphomagenic mechanisms and lymphoma-specific dependencies underlying defective *ATM*, we applied RNA sequencing and genome-scale loss-of-function clustered regularly interspaced short palindromic repeats (CRISPR)/Cas9 screens to systematically interrogate B-cell lymphomas arising in a novel murine model (*Atm*$^{-/-}$*nu*$^{-/-}$) with constitutional *Atm* loss, thymic aplasia but residual T-cell populations. *Atm*$^{-/-}$*nu*$^{-/-}$ lymphomas, which phenotypically resemble either activated B-cell-like or germinal center B-cell-like DLBCL, harbor a complex karyotype, and are characterized by MYC pathway activation. In *Atm*$^{-/-}$*nu*$^{-/-}$ lymphomas, we discovered nucleotide biosynthesis as a MYC-dependent cellular vulnerability that can be targeted through the synergistic nucleotide-depleting actions of mycophenolate mofetil (MMF) and the WEE1 inhibitor, adavosertib (AZD1775). The latter is mediated through a synthetically lethal interaction between RRM2 suppression and MYC dysregulation that results in replication stress overload in *Atm*$^{-/-}$*nu*$^{-/-}$ lymphoma cells. Validation in cell line models of human DLBCL confirmed the broad applicability of nucleotide depletion as a therapeutic strategy for MYC-driven DLBCL independent of *ATM* mutation status. Our findings extend current understanding of lymphomagenic mechanisms underpinning *ATM* loss and highlight nucleotide metabolism as a targetable therapeutic vulnerability in MYC-driven DLBCL.

Introduction

Dysregulation of the *MYC* proto-oncogene represents a fundamental mechanism underpinning pathogenesis in high-grade B-cell non-Hodgkin lymphoma (B-NHL).[1] In diffuse large B-cell lymphoma (DLBCL), the most com-

mon form of high-grade B-NHL,[2] *MYC* overexpression and chromosomal translocations, present in up to 40% and 20% of DLBCL respectively, confer inferior outcomes with standard rituximab-based chemoimmunotherapy.[3] Moreover, concurrent overexpression of MYC and BCL-2 defines double-expressor DLBCL,[4,5] while translocations of *MYC* with *BCL2* and/or *BCL6* characterize double/triple-hit lymphoma,[6,7] both associated with dismal prognosis and poor response to standard chemoimmunotherapeutic approaches.[4,5,7,8]

In addition to *MYC* disruption, recent next-generation sequencing efforts have revealed numerous other genomic events, unraveling a hitherto unrecognized level of genetic heterogeneity in DLBCL and other high-grade B-NHL.[9] Furthermore, besides acquired somatic alterations that fuel clonal evolution,[10] there is increasing recognition of germline genetic alterations as important predisposing factors for B-cell lymphomagenesis.[11] Understanding the therapeutic vulnerability associated with these genetic alterations is essential for devising novel therapeutic strategies with potential to improve clinical outcome. In this regard, the tumor suppressor gene ataxia-telangiectasia mutated (*ATM*) is recurrently mutated in 8-21% of sporadic DLBCL.[9,10,12,13] Moreover, high-grade B-NHL, particularly DLBCL, is the most frequent cancer type seen in individuals with ataxia-telangiectasia (A-T),[14,15] an inherited cancer predisposition syndrome caused by biallelic inactivating germline *ATM* mutations.[16] ATM plays a critical role in the maintenance of genome integrity through mediating DNA repair, cell cycle arrest and/or apoptosis in response to DNA double-strand breaks.[17] Beyond the DNA damage response, ATM participates in multifaceted cellular processes including regulation of chromatin remodeling, oxidative stress response, mitochondrial metabolism and autophagy.[17] Despite *in vivo* evidence substantiating the role of *ATM* loss as a driver of DLBCL,[18] its pathological consequence has not been fully elucidated. Moreover, little is known about the resultant cellular vulnerabilities that could be exploited for therapeutic targeting.

In order to address this issue, we combined RNA sequencing (RNA-seq) and genome-scale clustered regularly interspaced short palindromic repeats (CRISPR)/Cas9 screens to systematically interrogate pathogenic mechanisms and cellular dependencies within a novel murine model of DLBCL harboring constitutional *Atm* loss. We uncovered distinct transcriptional alterations associated with *Atm* loss that result in MYC activation and identified nucleotide biosynthesis among the actionable dependencies. We further demonstrated that nucleotide depletion induces a replication stress overload with resultant lethal effect that is dependent upon endogenous MYC overexpression in human DLBCL cells. Our findings thus unravel a novel mechanism underlying MYC dysregulation in *ATM*-defective DLBCL, providing a therapeutic approach for MYC-driven DLBCL and potentially other high-grade B-NHL that exploits nucleotide biosynthesis as a liability conferred by MYC dysregulation.

Methods

Details of assays performed according to established protocols are shown in the *Online Supplementary Appendix*.

Generation of *Atm*$^{-/-}$*nu*$^{-/-}$ mice

Animal studies were approved by the institutional ethics committee (AWERB) and conducted in accordance with UK Home Office regulations. The first mating of *Atm* heterozygote females (*Atm*$^{+/-}$*nu*$^{+/+}$; *129S6/SvEvTac-Atm*$^{tm1Aw-b}$*/J*, Jackson Laboratory, Maine, USA) with *Balb/c* nude males (*Atm*$^{+/+}$*nu*$^{-/-}$; Charles River, Harlow, UK) produced *Atm*$^{+/-}$*nu*$^{+/-}$ heterozygotes. Female *Atm*$^{+/-}$*nu*$^{+/-}$ progeny from the first generation underwent a second mating with male *Atm*$^{+/+}$*nu*$^{-/-}$ to obtain nude *Atm* heterozygotes (*Atm*$^{+/-}$*nu*$^{-/-}$). Finally, a third mating of second generation *Atm*$^{+/-}$*nu*$^{-/-}$ males with first generation *Atm*$^{+/-}$*nu*$^{+/-}$ females produced *Atm*$^{-/-}$*nu*$^{-/-}$ offspring.

Adoptive transfer of *Atm*$^{-/-}$*nu*$^{-/-}$ lymphomas and drug treatment

Lymphomas arising from *Atm*$^{-/-}$*nu*$^{-/-}$ mice (2x10^6 cells) were subcutaneously injected into NOD/LtSz-SCID/IL2γ^{tm1Wjl}/SzJ (NSG) mice (Charles River). Upon attaining average tumor volumes of 100 mm^3/mouse, mice were randomized into four oral gavage treatment arms receiving mycophenolate mofetil (MMF, 100 mg/kg/day; Selleckchem, Munich, Germany), adavosertib (AZD1775, 30 mg/kg/day; AstraZeneca, Cambridge, UK), combined MMF and AZD1775, or vehicle; respectively. Animals were euthanized when tumor volume exceeded 1,250 mm^3.

Cell lines

Cell lines were established without Epstein-Barr virus infection, by culturing single-cell suspensions of *Atm*$^{-/-}$*nu*$^{-/-}$ lymphomas (1x10^6), in RPMI containing 15% fetal calf serum, 1% pyruvate, 1% NEAA/β-mercaptoethanol (50 μM) and 1% penicillin/streptomycin (Life Technologies, Inchinnan, UK). Their immunophenotype and clonal relationship with the primary tumor were confirmed (*Online Supplementary Table S1*).

Human and Eμ-*Myc* cell lines were cultured according to standard protocols (see the *Online Supplementary Appendix*). Lymphoblastoid cell lines (LCL) were previously generated from samples obtained from A-T patients and healthy volunteers. Studies were approved by the West Midland, Coventry and Warwickshire Research Ethics Committee (REC: 20//WM/0098) and performed in accordance with local ethical guidelines. Written informed consent was obtained from all patients in accordance with the Declaration of Helsinki.

CRISPR/Cas9-mediated loss-of-function screen

Cell lines were modified to stably express *Cas9* and infected with the two-vector (lentiCas9-Blast and lentiGuide-Puro) lentiviral GeCKO v2.0 CRISPR knockout system (Addgene, MA) consisting of 130,209 pooled single-guide RNA (sgRNA) targeting 20,661 genes and 1,000 control sgRNA. Cells were cultured at optimal cell number (1-6x10^8) to maintain ≥1,000-fold coverage of the CRISPR sgRNA library. At day 0 and 18 (~14 doublings), DNA isolated from harvested viable cells was subjected to targeted deep sequencing of sgRNA using NextSeq HIGH 150 v2.5 kits on the NextSeq 500 sequencer (Illumina). The MAGeCK tool was used to determine sgRNA that were significantly depleted at day 18 compared to day 0 representing those targeting genes that were essential for cell survival ('hits').[19] KEGG pathway analysis was performed as for RNA-seq data.

Statistical analysis

Statistical analyses were performed using GraphPad Prism 9.2.0 (La Jolla, CA, USA).

Results

Atm$^{-/-}$*nu*$^{-/-}$ mice develop B-cell lymphomas with complex karyotype that closely model human activated B-cell-like and germinal center B-cell-like diffuse large B-cell lymphoma

In order to model B-NHL that results from constitutional *ATM* loss, we generated a novel athymic *Atm*-deficient

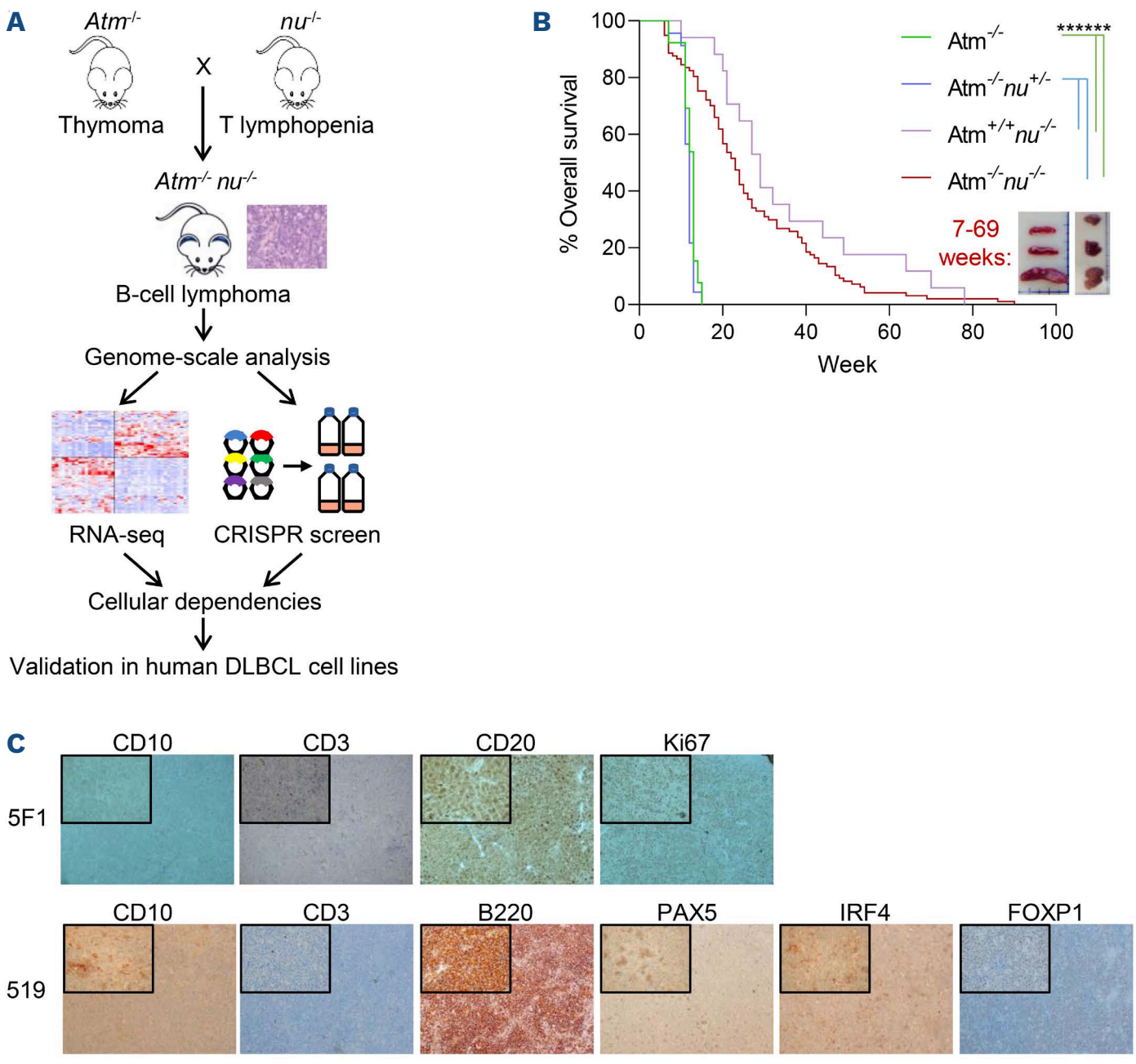

Figure 1. *Atm*$^{-/-}$*nu*$^{-/-}$ mice develop B-cell lymphomas that resemble human diffuse large B-cell lymphoma. (A) Schematic diagram summarizing experimental studies to characterize the *Atm*$^{-/-}$*nu*$^{-/-}$ murine model with the aim to identify therapeutic targets that can be translated to human B-cell non-Hodgkin lymphoma (B-NHL). (B) Kaplan-Meier curves displaying prolonged overall survival of *Atm*$^{-/-}$*nu*$^{-/-}$ (N=97) and *Atm*$^{+/+}$*nu*$^{-/-}$ (N=17) mice in comparison to *Atm*$^{-/-}$*nu*$^{+/-}$ (N=23) and *Atm*$^{-/-}$*nu*$^{+/+}$ (N=13) mice (P≤0.0001). Inset: *Atm*$^{-/-}$*nu*$^{-/-}$ littermates (7-69 weeks old) had enlarged spleens and livers in comparison to their *Atm*$^{+/+}$*nu*$^{+/+}$ and *Atm*$^{+/+}$*nu*$^{-/-}$ counterparts. (C) Immunohistology and morphology indicates that tumors from *Atm*$^{-/-}$*nu*$^{-/-}$ mice are lymphomas of B-cell origin resembling human diffuse large B-cell lymphoma (DLBCL). Representative images of sections (original magnification 10X and insets 40X) from two representative *Atm*$^{-/-}$*nu*$^{-/-}$ DLBCL (5F1, 519) stained with hematoxylin/eosin (H&E) as well as for B-cell (CD10, CD20, B220), T-cell (CD3), proliferation (Ki67, CD10) and DLBCL (PAX5, IRF4, FOXP1, CD10) markers are depicted. RNA-seq: RNA sequencing.

model (*Atm*$^{-/-}$*nu*$^{-/-}$) (Figure 1A). This overcomes an inherent limitation with *Atm*$^{-/-}$ mice which develop lethal thymoma in early life (<16 weeks) precluding their use to study B-cell lymphomagenesis.[20,21]

Crossing *Atm*$^{-/-}$ mice with *nu*$^{-/-}$ mice prevented thymoma development, leading to prolonged survival of *Atm*$^{-/-}$*nu*$^{-/-}$ mice, irrespective of whether death was caused by tumor or other causes, mostly infection (median survival 13 *vs.* 23 weeks for *Atm*$^{-/-}$ *vs.* *Atm*$^{-/-}$*nu*$^{-/-}$ mice) (Figure 1B; *Online Supplementary Figure S1*). *Atm*$^{-/-}$*nu*$^{-/-}$ mice instead developed B-NHL, reminiscent of patients with A-T.[14,15] B-cell lymphomas emerged with 24% penetrance, manifesting in splenomegaly, frequent hepatomegaly and nodal involvement that arose at a median of 25 weeks (range, 7-69) (Figure 1B). These lymphomas histologically and immunophenotypically resembled human DLBCL, with 6 of 14 lymphomas demonstrating Ki67 >50%, and harboring identifiable clonal *IGHV-D-J* gene rearrangements (Figure 1C; *Online Supplementary Table S1*).

B-cell lymphomagenesis in the context of constitutional *ATM* loss has also been recapitulated by the ATMKO.CD3εKO model generated by interbreeding *Atm*-deficient mice with CD3ε-knockout mice.[18] However, unlike the ATMKO.CD3εKO model wherein T-cell immunity is absent,[18] T cells are present in the *Atm*$^{-/-}$*nu*$^{-/-}$ model, albeit at markedly reduced level (Figure 2A), akin to patients with A-T.[22] Early progenitor B-cell number retention (B220^{+}CD43^{+}) coupled with a trend towards reduced levels of more mature B-cell populations in the bone marrow (Figure 2A) and spleen (*data not shown*) in the *Atm*$^{-/-}$*nu*$^{-/-}$ model resembles A-T patients impaired B-cell development.[16] Moreover, in contrast to ATMKO.CD3εKO mice which were unable to form germinal centers and exclusively developed lymphomas resembling ABC DLBCL,[18] germinal centers were preserved in *Atm*$^{-/-}$*nu*$^{-/-}$ mice (Figure 2B). While the majority of *Atm*$^{-/-}$*nu*$^{-/-}$ lymphomas displayed gene expression signatures characteristic of human ABC DLBCL, some resembled GCB DLBCL (Figure 2C; *Online Supplementary Figure S2A, B*).[23,24] *Atm*$^{-/-}$*nu*$^{-/-}$ mice therefore developed lymphomas that reflect the spectrum of DLBCL observed in patients harboring defective *ATM*.[9,13,24] *Atm*$^{-/-}$*nu*$^{-/-}$ lymphomas exhibited a diverse landscape of complex karyotypic alterations (mean 10; range, 5-17) indicating substantial intertumoral and intratumoral genetic heterogeneity (Figure 2D; *Online Supplementary Figure S2C*). These alterations included chromosomal translocations and whole chromosome gains and losses, with the majority being subclonal. As found in human DLBCL,[25] *IgH* and *Myc* alterations were evident with *Myc* duplication present in two of six *Atm*$^{-/-}$*nu*$^{-/-}$ lymphomas (*Online Supplementary Figure S2C*; *Online Supplementary Table S2*). These features suggest a high level of genomic instability and clonal evolution in *Atm*$^{-/-}$*nu*$^{-/-}$ lymphomas likely driven in part by *Atm*

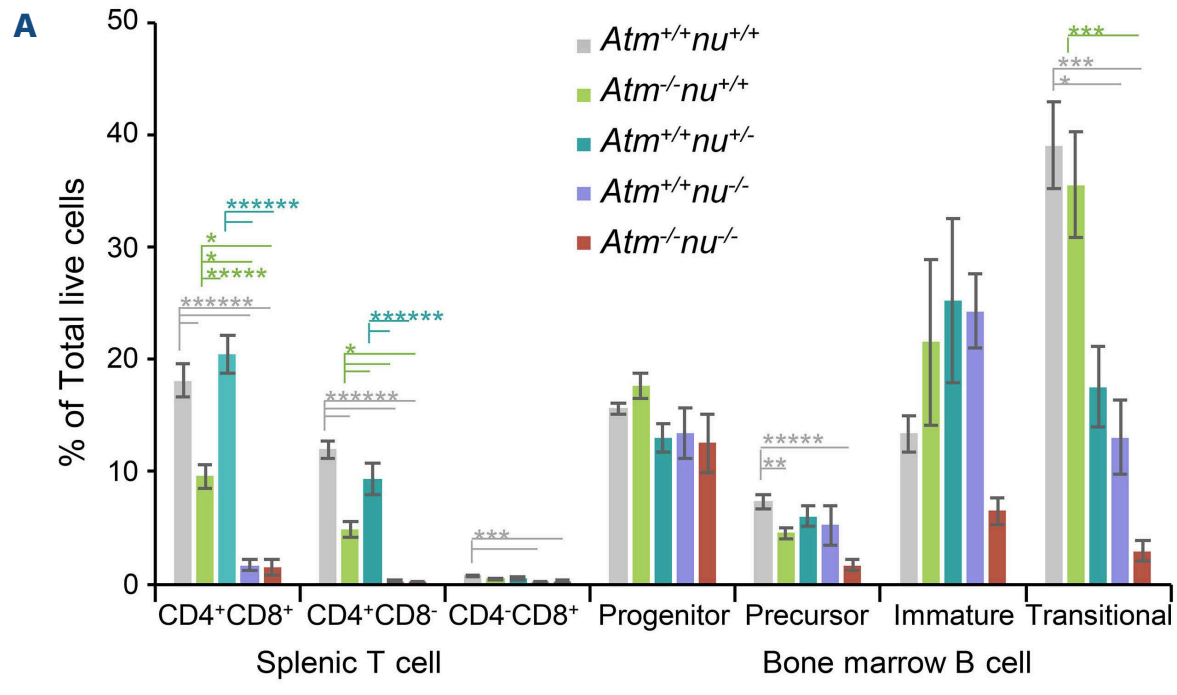

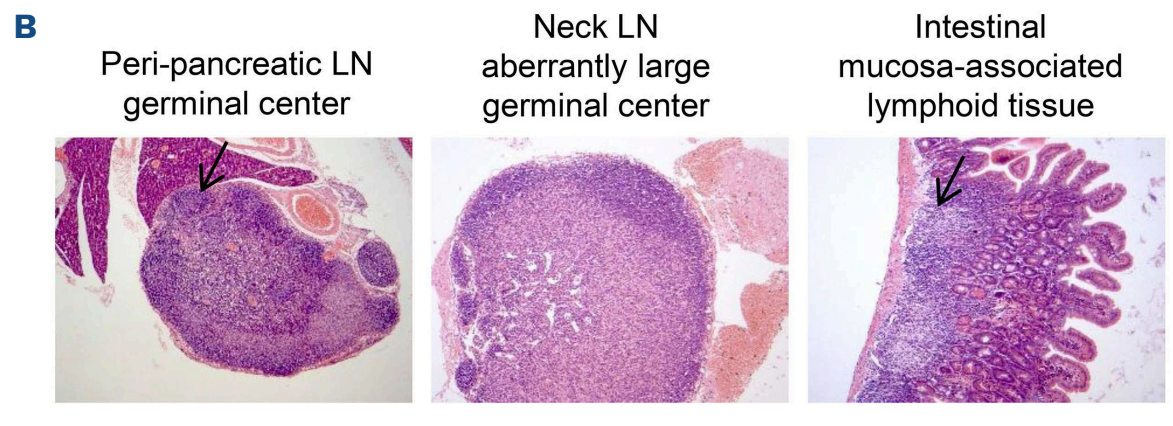

Continued on following page.

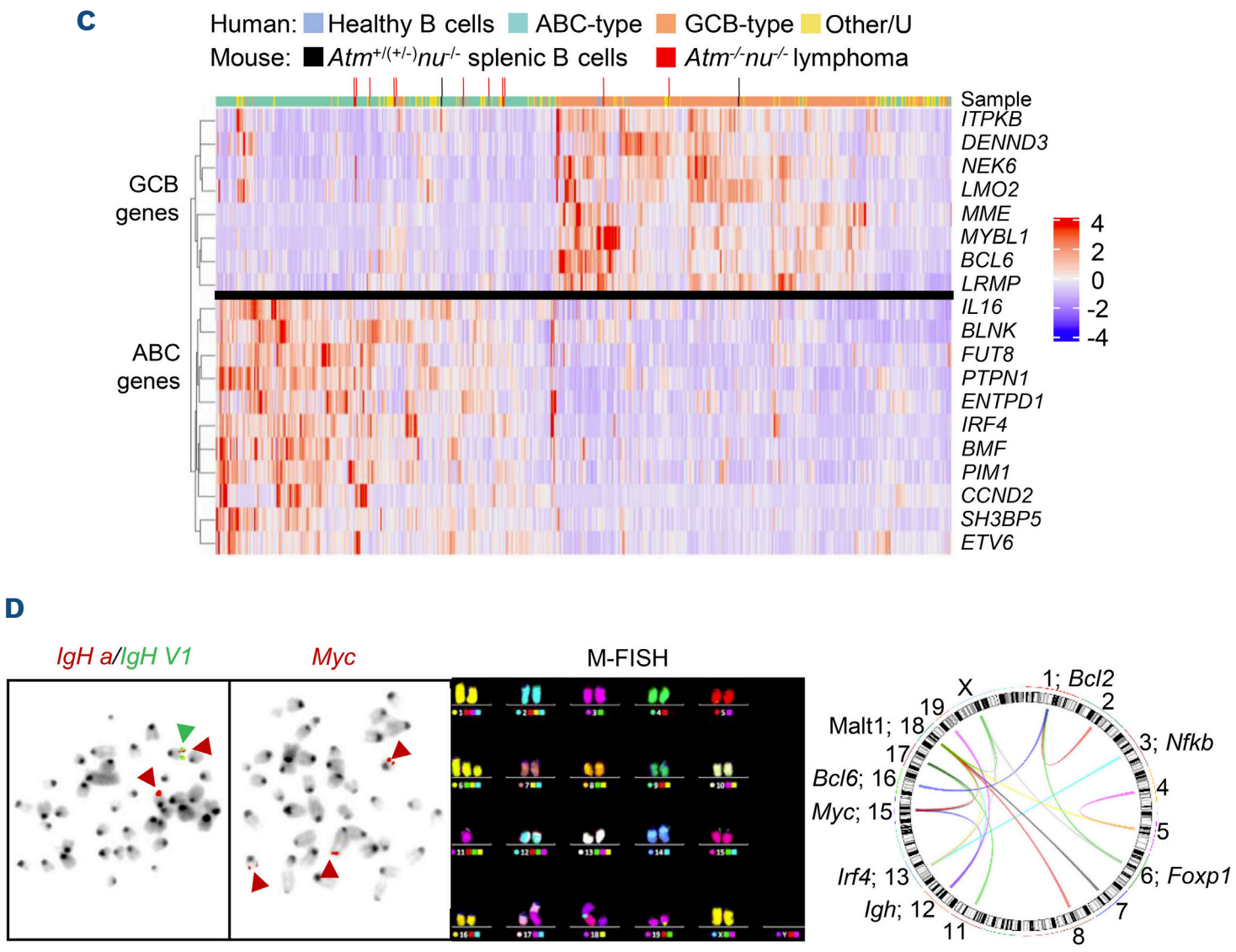

Figure 2. B-cell lymphomas that develop in *Atm*$^{-/-}$*nu*$^{-/-}$ mice have a complex karyotype that resembles human activated B-cell-like and germinal center B-cell-like diffuse large B-cell lymphoma. (A) Fluorescence-activated cells sorting analysis of splenic T-cell and bone marrow B-cell populations of 6-8-week-old mice revealed reduced but not completely absent T-cell populations in *Atm*$^{+/+}$*nu*$^{-/-}$ (N=4) and *Atm*$^{-/-}$*nu*$^{-/-}$ (N=5) mice compared to *Atm*$^{+/+}$*nu*$^{+/+}$ (N=16), *Atm*$^{-/-}$*nu*$^{+/+}$ (N=19) and *Atm*$^{+/+}$*nu*$^{+/-}$ (N=6). T cells were arrested at the CD3^{+}CD8^{+} and CD3^{+}CD4^{+} differentiation stage. Significantly fewer precursor (B220^{+}CD43^{-}) and transitional (B220^{high}-CD43^{-}IgM^{+}) B cells were evident in the bone marrow of *Atm*$^{-/-}$*nu*$^{-/-}$ mice compared to their *Atm*$^{+/+}$*nu*$^{+/+}$ and/or *Atm*$^{-/-}$*nu*$^{+/+}$ counterparts, whilst the levels of progenitor (B220^{+}CD43^{+}) B cells were similar across all genotypes. Immature (B220^{med}CD43^{-}IgM^{+}) B-cell levels were highly variable even within genotypes. Data are presented as mean ± standard error of the mean. Statistical significance, ascertained by one-way ANOVA with Tukey *post hoc* test, is denoted by: $^{*}P\leq0.05$, $^{**}P\leq0.01$, $^{***}P\leq0.005$, $^{****}P\leq0.001$, $^{*****}P\leq0.0005$, $^{******}P\leq0.0001$. (B) Germinal centers (arrows); albeit with perturbed morphology and larger than normal; were evident in various lymph nodes (LN) and gut mucosa of *Atm*$^{-/-}$*nu*$^{-/-}$ mice. Representative images of sections (original magnification: 5X, pancreas; 10X, neck, intestine) stained with hematoxylin/eosin (H&E) are depicted. (C) Comparison of RNA-sequencing (RNA-seq) data of *Atm*$^{-/-}$*nu*$^{-/-}$ lymphomas (N=11) and control splenic B-cells from *Atm*$^{+/+}$*nu*$^{-/-}$ and *Atm*$^{+/-}$*nu*$^{-/-}$ mice (N=2) against published RNA-seq datasets of human activated B-cell-like (ABC) DLBCL and healthy control germinal center B cells (GCB)[55,56] suggests that the majority of *Atm*$^{-/-}$*nu*$^{-/-}$ lymphomas cluster with human ABC DLBCL.[9] (D) Left panel: specific translocations involving *IgH* and *Myc* were assessed by M-fluorescence *in situ* hybridization (FISH) in six *Atm*$^{-/-}$*nu*$^{-/-}$ lymphomas. The representative example shown (5F3) harbored *Myc* gain and *IgH* loss as indicated by the arrows (*IgHα*, red; *IgHVi*, green; *Myc*, red). Right panel: the circos plot summarizing the chromosomal alterations for the 6 *Atm*$^{-/-}$*nu*$^{-/-}$ B-cell lymphomas revealed an absence of common translocations. Chromosomes are indicated by the numerals and annotated with lymphoma relevant genes localized in the regions affected by chromosomal alterations.

loss. Taken together, our *Atm*$^{-/-}$*nu*$^{-/-}$ mice provide a robust model for the elucidation of pathogenic mechanisms and therapeutic targets in human DLBCL.

Atm$^{-/-}$*nu*$^{-/-}$ lymphomas are characterized by MYC activation

In order to decipher the biological processes underlying B-cell lymphomagenesis in *Atm*$^{-/-}$*nu*$^{-/-}$ mice, we characterized the transcriptomic landscape of *Atm*$^{-/-}$*nu*$^{-/-}$ lymphomas. RNA-seq data revealed 1,493 upregulated and 1,010 downregulated genes in *Atm*$^{-/-}$*nu*$^{-/-}$ lymphomas relative to healthy splenic B cells from *Atm*$^{+/+}$*nu*$^{-/-}$ and *Atm*$^{+/-}$*nu*$^{-/-}$ mice (Figure 3A; *Online Supplementary Table S3*).

Genes involved in cell cycle progression (e.g., *Ccnf, Cdk6*, *Ccnb1, Cdca5*), mitosis (e.g., *Klhl13*, *Psrc1*, *Spdl1*, *Kifc1*), DNA replication (e.g., *Orc1*, *Mcm6*, *Pole, Prim1, Rfc4*) and cellular metabolism (e.g., *Mgll, Gpt2, Uqcr10, Cox4i2*) were among the most significantly upregulated in *Atm*$^{-/-}$*nu*$^{-/-}$ lymphomas (Figure 3B; *Online Supplementary Table S4*), reflecting the loss of ATM-dependent cell cycle checkpoints and

resultant high proliferation rate. Concurrently, key genes mediating homologous recombination repair (e.g., *Rad51, Brca1, Pole*), chromatin modification (e.g., *Ezh2, Cenpa*), replication stress response (e.g., *Wee1, Chk1*) and nucleotide biosynthesis (e.g., *Rrm2, Tyms*) were some of the most significantly overexpressed. Finally, reflecting the malignant properties of transformed B cells in *Atm*$^{-/-}$*nu*$^{-/-}$ mice, tumor suppressor genes (e.g., *Txnip, Cul9*) and genes involved in normal B-cell development, signaling and activation (e.g., *Cr2, Akt3, Icosl, Cx3cr1*) as well as antigen presentation (e.g., *Cd1d1*) were significantly downregulated, whereas genes that promote tumor immune evasion (e.g. *Ctla4*) were upregulated (*Online Supplementary Tables S4, S5*).

An association between ATM loss, aberrant gene rearrangements and MYC deregulation has been previously established.[26] Moreover, ATM-dependent DNA damage response counteracts the tumorigenic effect of MYC activation, providing the basis for co-operation between ATM and MYC during tumorigenesis.[27-29] Concurring with this notion and the presence of *Myc* duplications in *Atm*$^{-/-}$*nu*$^{-/-}$ lymphomas, gene set enrichment analysis (GSEA) analysis of RNA-seq data demonstrated that MYC targets, and MYC-induced E2F targets, were among the most enriched gene sets in these lymphomas (Figure 3C, D; *Online Supplementary Figure S3A, B*; *Online Supplementary Table S6*), which was consistent with elevated MYC protein expression (Figure 3E; *Online Supplementary Figure S3C*). As replication stress is a principal consequence of MYC dysregulation,[30] upregulation of replication stress response genes in *Atm*$^{-/-}$*nu*$^{-/-}$ lymphomas may be a consequence of upregulated MYC in the majority of these lymphomas. Other drivers, such as those involved in repair of DNA lesions induced by MYC-driven replication stress, may also play a role.[31] The transcriptomic landscape of *Atm*$^{-/-}$*nu*$^{-/-}$ lymphomas thus identified potentially targ-

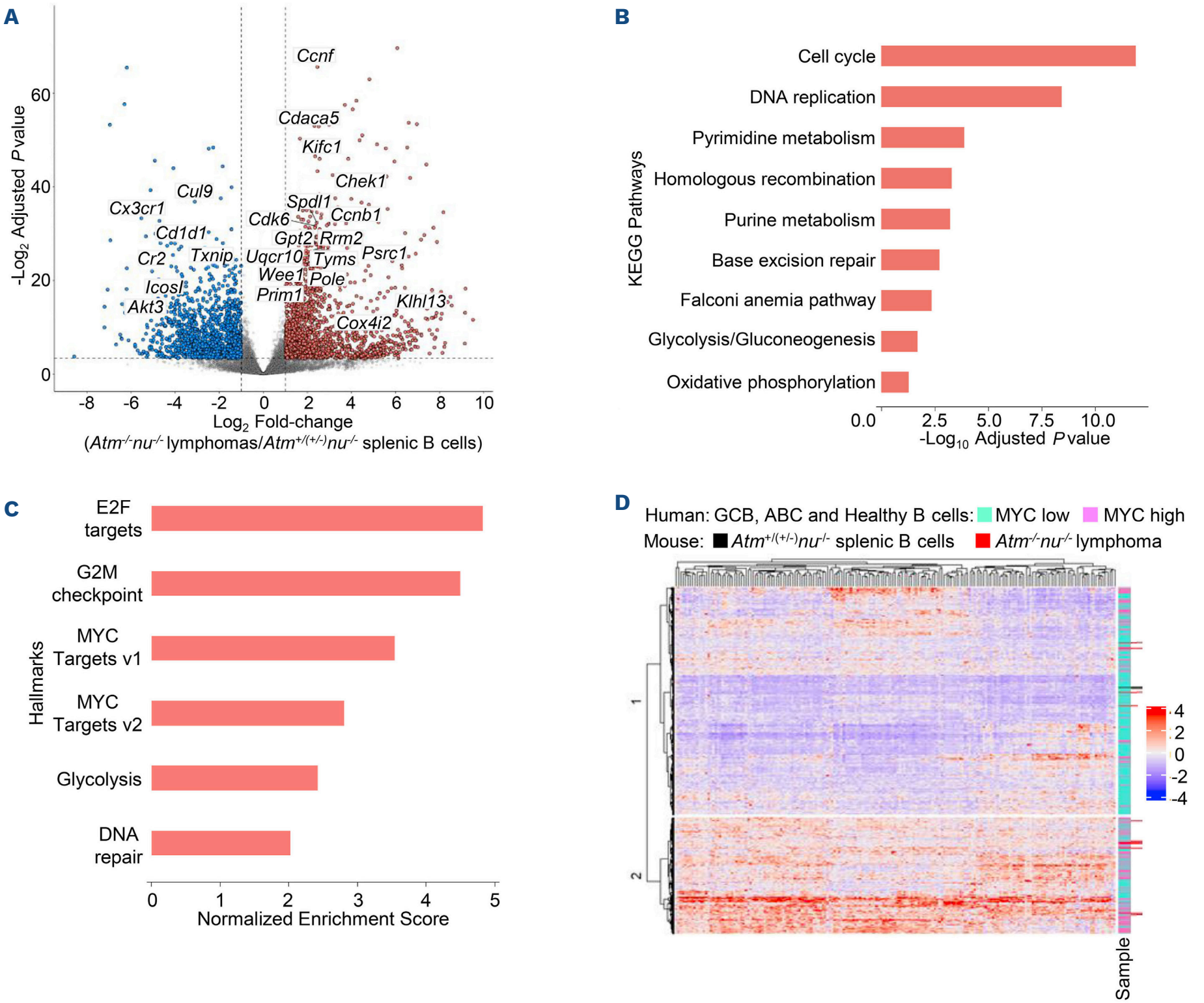

Continued on following page.

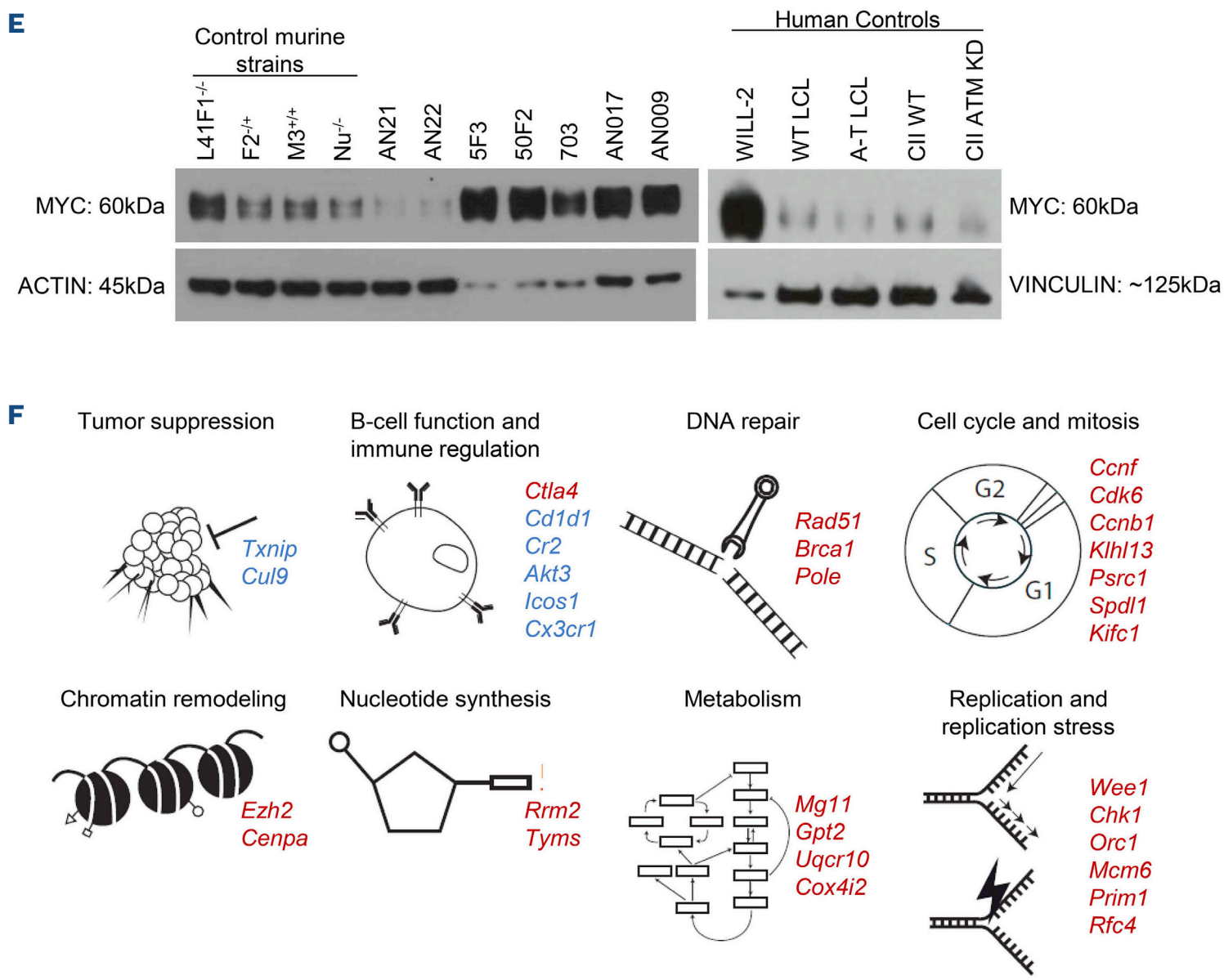

Figure 3. *Atm*$^{-/-}$*nu*$^{-/-}$ lymphomas display a transcriptional profile characterized by MYC activation. (A) RNA-sequencing (RNA-seq) analysis of *Atm*$^{-/-}$*nu*$^{-/-}$ lymphomas (N=11) and control splenic B cells from *Atm*$^{+/+}$*nu*$^{-/-}$ and *Atm*$^{+/-}$*nu*$^{-/-}$ mice (N=2) revealed differentially expressed genes in *Atm*$^{-/-}$*nu*$^{-/-}$ lymphomas; 1,493 upregulated (red) and 1,010 downregulated (blue). (B, C) Biological processes that are the most significantly upregulated in *Atm*$^{-/-}$*nu*$^{-/-}$ lymphomas compared to control splenic B cells as revealed by (B) Kyoto Encyclopedia of Genes and Genomes (KEGG) pathway and (C) gene set enrichment analysis (GSEA) hallmark pathway analyses. (D) Comparison of the murine RNA-seq data to human activated B-cell-like (ABC) (N=252), germinal center B cells (N=278) and unknown (N=94) DLBCL;[9] stratified according to MYC target gene expression: MYC high (N=201) and low (N=436)[57] reveals that a high proportion of *Atm*$^{-/-}$*nu*$^{-/-}$ lymphomas align with high MYC-expressing human diffuse large B-cell lymphoma (DLBCL). (E) MYC expression is upregulated in the majority of *Atm*$^{-/-}$*nu*$^{-/-}$ lymphomas (5F3, 50F2, 703, AN017, AN009) in comparison to murine basal controls: M3$^{+/+}$ (*Atm*$^{+/+}$*nu*$^{+/+}$), Nu$^{-/-}$(*Atm*$^{+/+}$*nu*$^{-/-}$), F2$^{-/+}$ (*Atm*$^{-/+}$*nu*$^{+/+}$); MYC positive control: L41F1$^{-/-}$(*Atm*$^{-/-}$*nu*$^{+/+}$); and also human ATM isogenic CII chronic lymphocytic leukemia (CLL) cell lines, LCL derived from healthy and ataxia-telangiectasia (A-T) individuals with WILL-2 (human DLBCL) as a MYC-positive control on a separate gel. (F) Summary of the most relevant significantly upregulated (red) and downregulated (blue) genes and biological processes in *Atm*$^{-/-}$*nu*$^{-/-}$ lymphomas.

etable biological features, including DNA repair, a requirement for nucleotide biosynthesis due to replicative stress, and dysregulated MYC that likely underpin *ATM*-defective DLBCL oncogenesis (Figure 3F).[32-35]

Genome-wide CRISPR/Cas9 screen identifies nucleotide biosynthesis as a cellular dependency of *Atm*$^{-/-}$*nu*$^{-/-}$ lymphomas

We hypothesized that in a significant number of these lymphomas, heightened replication stress, due in part to MYC upregulation, could render these tumors dependent upon nucleotide biosynthesis. In order to systematically identify potentially actionable lymphoma-specific dependencies within our *Atm*$^{-/-}$*nu*$^{-/-}$ model, we performed a genome-scale CRISPR/Cas9-mediated loss-of-function screen on two *Atm*$^{-/-}$*nu*$^{-/-}$ lymphoma-derived cell lines (50F2 and AN017) (Figure 4A).

At the optimal false discovery rate (FDR)-adjusted *P* value threshold of 0.05 that produced a manageable gene output, 1,000 and 340 hits were identified in 50F2 and AN017 respectively, with 197 hits common to both (Figure 4B, C; *Online Supplementary Table S7*). Consistent with the observed MYC dysregulation, analysis of depleted sgRNA revealed a *Myc* dependency (rank 861; fold change: -0.742) as well as dependency on key biological processes common to both cell lines (Figure 4D, E; *Online Supplementary Figure S4*; *Online Supplementary Table S8*). These included genes involved in DNA repair (e.g., *Parp1*, *Rad50*, *Rad51*, *Rnaseh2c*,

Mcm7), DNA replication (e.g., *Pold2*, *Mcm7*, *Rnaseh2c*), telomere maintenance (e.g., *Pot1*, *Telo2*) and cell cycle regulation (e.g., *Cdk6*, *Fam58b*), consistent with cellular dependence on alternative genome maintenance regulators upon *Atm* loss. Notably, the top hits identified from the CRISPR/Cas9 screen were also highly enriched in genes mediating nucleotide biosynthesis, including those encoding for the enzymes *Tyms*, *Umps*, *Cmpk1*, *Cad* and *Ppat* that play key roles in deoxynucleotide triphosphate (dNTP) production, as well as other important components within the purine biosynthesis pathway (Figure 4F, G). These observations therefore support the notion that both *Myc* activity and nucleotide biosynthesis are major cellular dependencies of *Atm*$^{-/-}$*nu*$^{-/-}$ lymphomas.

Nucleotide depletion induces replication stress overload and tumor-specific lethality in MYC-dependent *Atm*$^{-/-}$*nu*$^{-/-}$ lymphomas

The identification of MYC and nucleotide biosynthesis as cellular dependencies, together with evidence for their upregulation as part of a heightened replication stress response, raises the question of whether these lymphomas are sensitive to MYC inhibition and depletion of cellular nucleotide pools through inhibition of nucleotide biosynthesis. To address this, we examined the effect of MMF, an inhibitor of *de novo* purine biosynthesis,[36] on *Atm*$^{-/-}$*nu*$^{-/-}$ lymphomas. Moreover, since *Wee1* and *Rrm2* were among the most significantly overexpressed genes in *Atm*$^{-/-}$*nu*$^{-/-}$ lymphomas, we also evaluated the effect of the WEE1 inhibitor, AZD1775, which can promote degradation of RRM2, a subunit of ribonucleotide reductase that is essential for dNTP biosynthesis.[37]

In vitro MYC inhibition of an *Atm*$^{-/-}$*nu*$^{-/-}$ lymphoma-derived cell line conferred significant cytotoxicity (Figure 5A). Furthermore, treatment of three *Atm*$^{-/-}$*nu*$^{-/-}$ lymphoma-derived cell lines with physiologically achievable concentrations of MMF or AZD1775 resulted in dose-dependent cytotoxicity, which was rescued via MYC inhibition (AZD) or addition of exogenous dNTP (MMF), consistent with the increased requirement for nucleotide biosynthesis caused by MYC activation (Figure 5B-D). Notably, MMF and AZD1775-induced cytotoxicity was also attained in *Atm* wild-type, Eμ-*Myc*-driven tumors that resemble human Burkitt lymphoma (*Online Supplementary Figure S5A*).[38]

We reasoned that nucleotide depletion to catastrophic levels through concerted actions of MMF and AZD1775 in *Atm*$^{-/-}$*nu*$^{-/-}$ lymphomas might enhance lethality. Indeed, AZD1775 was synergistic when used in combination with MMF (Figure 5B, E), which was reversible upon MYC inhibition, dNTP supplementation or RRM2 upregulation via the specific NEDD8 inhibitor (NEDDi), pevonedistat (Figure 5C, D, F). As expected, AZD1775 treatment led to attenuated RRM2 levels in *Atm*$^{-/-}$*nu*$^{-/-}$ lymphoma cells and a derived-cell line (50F2) and activation of the replication stress response (Figure 5G; *Online Supplementary Figure S5B*). The latter was evidenced by the induction of CHK1 phosphorylation, consistent with the exacerbation of replication stress upon nucleotide depletion.

In order to confirm the *in vivo* efficacy of nucleotide depletion as a therapeutic strategy, administration of MMF and AZD1775, alone or combined, to mice engrafted with an

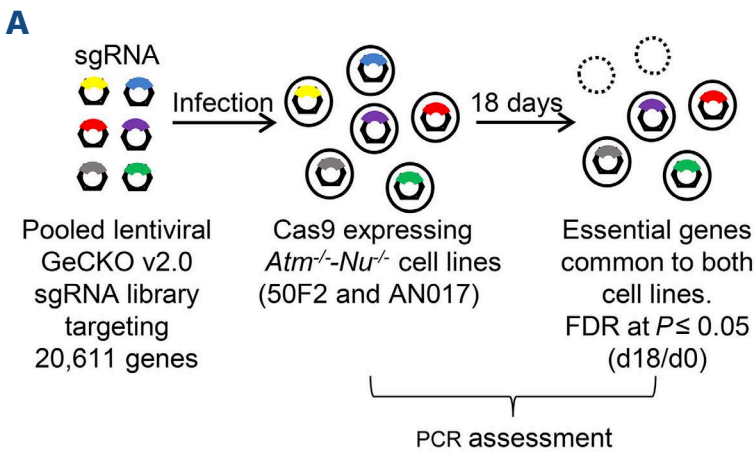

Continued on following page.

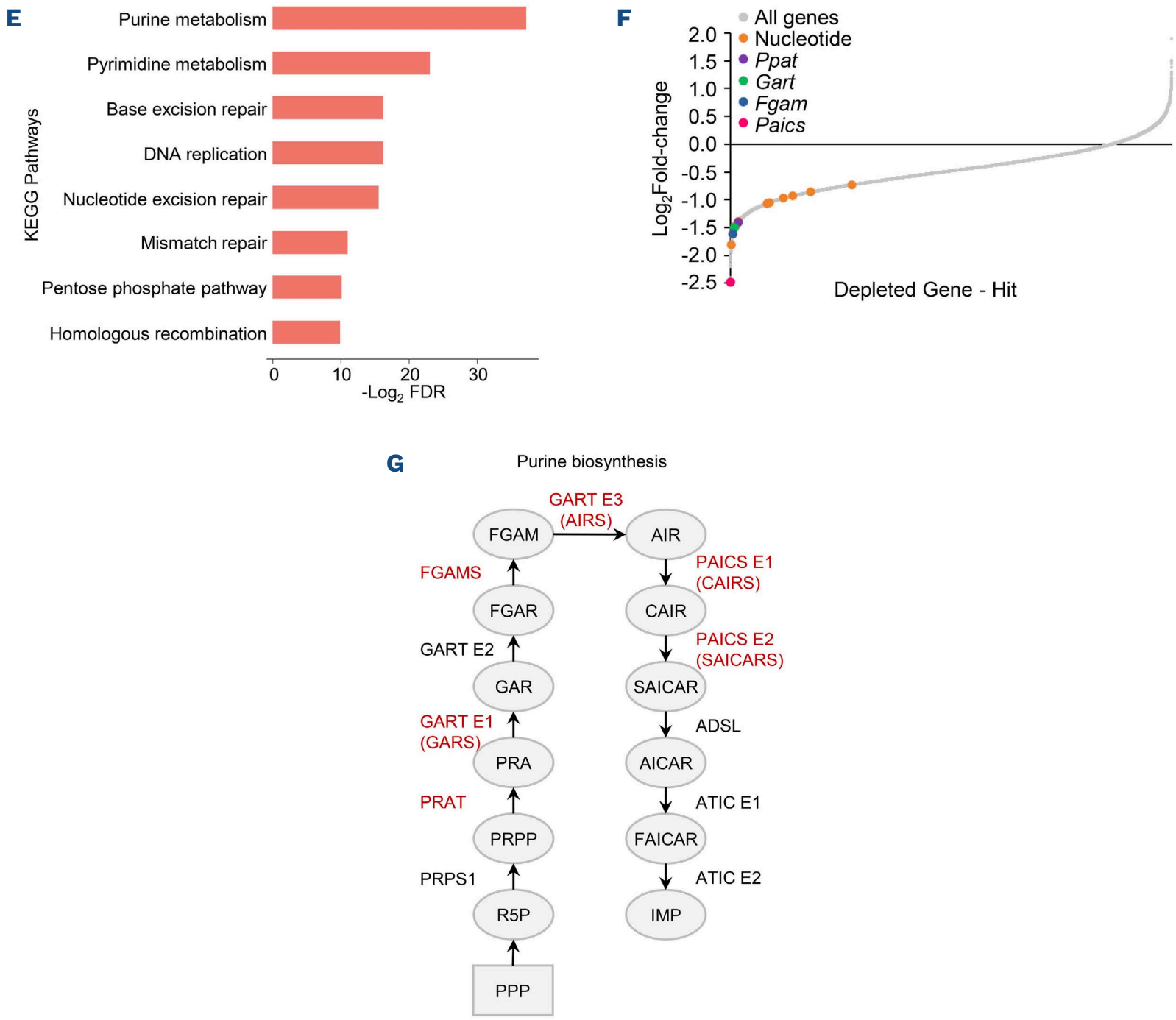

Figure 4. Genome-wide CRISPR/Cas9 screen identifies nucleotide biosynthesis as a cellular dependency of *Atm*$^{-/-}$*nu*$^{-/-}$ lymphomas. (A) Identification of cellular dependencies by genome-scale clustered regularly interspaced short palindromic repeats (CRISPR)/Cas9-mediated loss-of-function screens of 2 cell lines established from *Atm*$^{-/-}$*nu*$^{-/-}$ lymphomas (50F2 and AN017). (B) Cumulative number of hits (from 21,513 potential genes) at various false discovery rates (FDR) in each individual cell line and common to both (combined). A 5% FDR (FDR <0.05) was set for all further analysis. (C) The number of mutually exclusive and common hits between the 2 cell lines at FDR <0.05. (D) Major biological processes represented by the discovered hits from the CRISPR/Cas9 screen. These processes were also upregulated in *Atm*$^{-/-}$*nu*$^{-/-}$ lymphomas as evidenced from RNA-sequencing data. (E) KEGG pathway analysis of hits common to both *Atm*$^{-/-}$*nu*$^{-/-}$ lymphoma cell lines revealing essential cellular dependencies. (F, G) Hits identified within the purine biosynthesis pathway (dark orange), the most significantly affected biological process, that represent potential therapeutic targets. sgRNA: single guide RNA.

Atm$^{-/-}$*nu*$^{-/-}$ lymphoma (AT15c) was well-tolerated. Combined treatment significantly reduced tumor volume and delayed tumor growth as none of the tumors attained the maximum permitted tumor volume within this treatment group (Figure 5H).

The cytotoxicity of the nucleotide biosynthesis inhibitors was exerted via apoptosis (Figure 6A, B). This is likely due to replication stress overload as evidenced by impeded replication fork progression, resulting in fork stalling with compensatory initiation of nearby dormant origins upon combined MMF and AZD1775 treatment (Figure 6C).[39,40] The latter is supported by the retention of *Atm*$^{-/-}$*nu*$^{-/-}$ lymphoma cells in quiescent S-phase with the accumulation of partially-replicated DNA and lethal DNA damage (Figure 6D-F; *Online Supplementary Figure S5C*).[41] Our observations in *Atm*$^{-/-}$*nu*$^{-/-}$ lymphomas therefore provided conceptual proof of nucleotide depletion as a viable therapeutic strategy for DLBCL harboring *MYC* dysregulation associated with *ATM* loss.

MYC overexpression broadly sensitizes human diffuse large B-cell lymphoma cells to nucleotide depletion with AZD1775

Human DLBCL may exhibit *MYC* dysregulation concurrently with *ATM* disruption.[9] However, the majority of DLBCL with

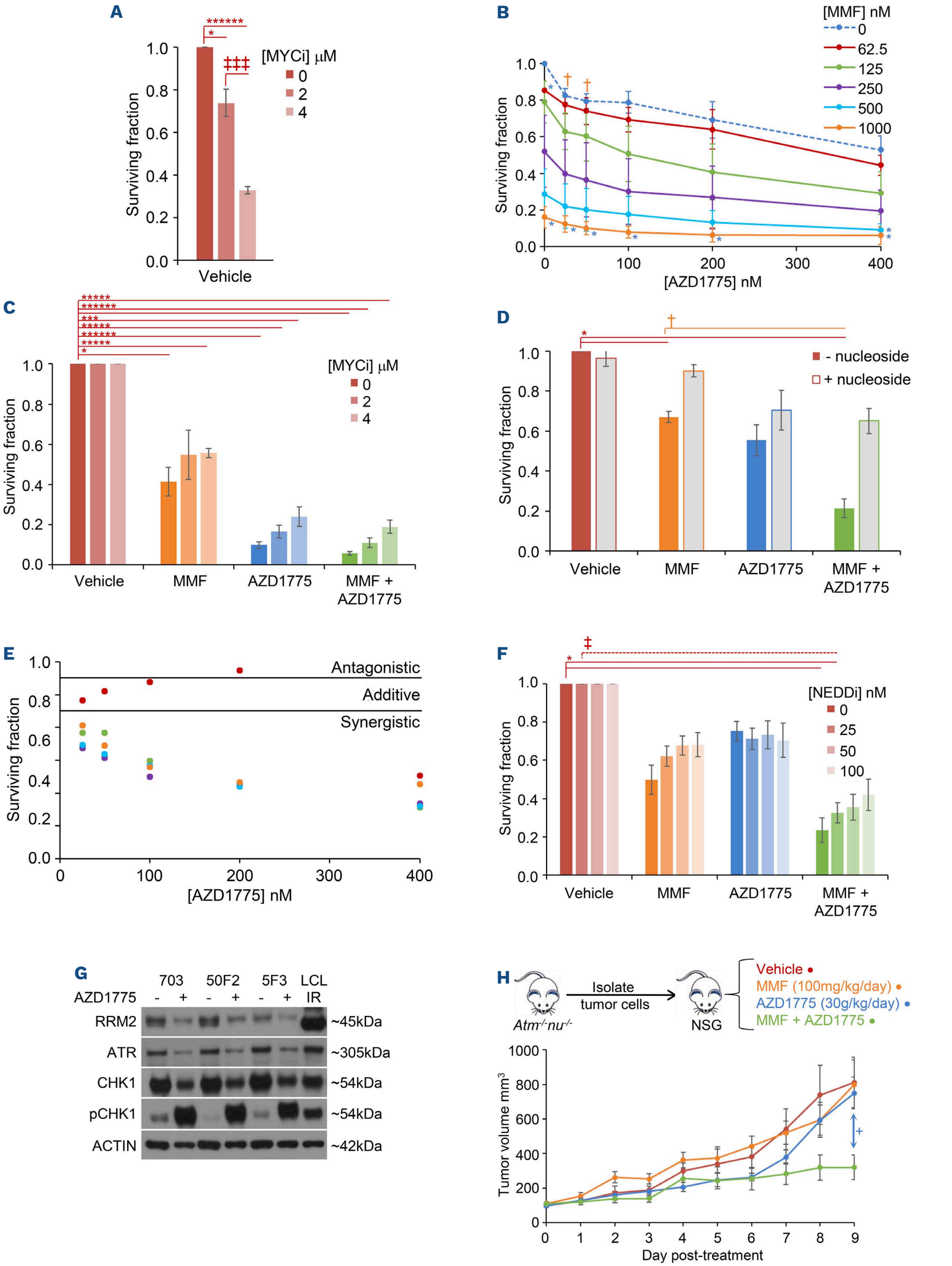

Continued on following page.

Figure 5. Nucleotide depletion induces replication stress overload and lethality in MYC-dependent *Atm*$^{-/-}$*nu*$^{-/-}$ lymphomas. (A) Exposure for 72 hours (h), of the *Atm*$^{-/-}$*nu*$^{-/-}$ lymphoma cell line, 50F2, to a MYC inhibitor (MYCi, MYCi361); at doses reported (Selleckchem) to specifically inhibit MYC activity; led to significant toxicity as measured by CellTitre-Glo assay. (B-D) Exposure of *Atm*$^{-/-}$*nu*$^{-/-}$ lymphoma cell lines (703, 5F3, 50F2) to mycophenolate mofetil (MMF) and/or adavosertib (AZD1775) for 72 h led to significant toxicity as measured by (B) Alamar Blue, (C) CellTitre-Glo or (D) propidium iodide (PI) exclusion that could be rescued by (C) inhibition of MYC or (D) addition of exogenous nucleosides. (C) Surviving fraction was normalized to the appropriate MYCi dose to highlight any rescue from MMF and/or AZD1775 toxicity. (E) Combining MMF and AZD1775 results in synergistic cytotoxicity. (F) The cytotoxic effect of MMF and AZD1775 can be ameliorated by upregulation of RRM2 via NEDD8 inhibition (MLN4924, pevonedistat). (C, D, F) Cell lines were treated with MMF doses corresponding to the half maximal effective concentration (EC_{50}) and 400 nM AZD1775. (G) AZD1775 (400 nM; 72 h) exerts its effects via depletion of RRM2 and subsequent exacerbation of replication stress, on an Atm-deficient background, via reduction of ATR-mediated DNA repair activity in *Atm*$^{-/-}$*nu*$^{-/-}$ lymphoma cell lines. Irradiated (IR, 6 Gy, 30 minutes) A-T patient-derived lymphoblastoid cell lines (LCL) serve as a positive control. (H) Nucleotide depletion with AZD1775 and MMF demonstrated significant activity *in vivo*. NSG mice harboring adoptively transferred *Atm*$^{-/-}$*nu*$^{-/-}$ lymphoma (AT15c) were administered vehicle (N=4), MMF (100 mg/kg; N=5), AZD1775 (30 mg/kg; N=5), or a combination of MMF and AZD1775 (N=6) via oral gavage for 7 days. Overall tumor size was significantly smaller in animals receiving combination therapy, in comparison to AZD1775 alone. Data are presented as mean ± standard error of the mean of (A, C) 50F2, (B, D, F) the 3 cell lines (703, 5F3, 50F2) or (H) mice per treatment arm. All cytotoxicity experiments were performed at least in quadruplicate. Statistical significance *versus* vehicle (*), MMF (†), AZD1775 (+), MYCi, nucleoside or NEDDi (‡), was ascertained by matched multi-comparison (A) one-way or (B, C, D, F, H) two-way ANOVA with Tukey *post hoc* test denoted by: $^{*}P\leq0.05$, $^{**}P\leq0.01$, $^{***}P\leq0.005$, $^{****}P\leq0.001$, $^{*****}P\leq0.0005$, $^{******}P\leq0.0001$.

MYC overexpression do not exhibit *ATM* loss.[9,13,42] In order to determine whether the use of nucleotide depletion as a therapeutic strategy can be broadly extended to human DLBCL harboring *MYC* dysregulation associated with pathogenic mechanisms beyond *ATM* loss, we set out to validate such a therapeutic strategy within these contexts.

Human DLBCL cell lines were sensitive to MYC inhibition and physiologically achievable doses of MMF and AZD1775, which for AZD1775, correlated with MYC upregulation (Figure 7A-C; *Online Supplementary Figures S3C* and *S6A, B*). Similar to *Atm*$^{-/-}$*nu*$^{-/-}$ lymphomas, synergism was evident upon AZD1775 and MMF co-treatment particularly in high MYC-expressing cell lines (Figure 7C, D; *Online Supplementary Figure S6A*), with MYC inhibition reducing cytotoxicity (Figure 7E). In contrast, loss of ATM did not impact upon MMF or AZD1775 sensitivity in A-T patient-derived LCL cells nor in CLL-derived CII cells with ATM knockdown (*Online Supplementary Figure S6C, D*). Moreover, the ATM-deficient DLBCL cell line (Farage) was AZD1775-resistant (Figure 7C; *Online Supplementary Figure S6A, E*). Upon mining the Cancer Dependency Map (DepMap)[43] data that uncovers gene dependencies in hundreds of cancer cell lines we observed a significant inverse correlation between protein expression of two nucleotide biosynthesis genes (CAD, UMPS) and MYC, but not ATM (Figure 7F). In addition, mining published human DLBCL RNA-seq datasets revealed that, compared to germinal center B cells (GCB), ABC DLBCL concurrently express significantly reduced *ATM* and elevated *MYC* levels. Furthermore, *MYC* expression is higher in the ABC than the GCB DLBCL cohort whilst expression of a purine/pyrimidine biosynthesis gene-set is elevated in ABC DLBCL in comparison to both GCB DLBCL and GCB (*Online Supplementary Figure S6F*). Thus, nucleotide biosynthesis inhibition may be particularly relevant for an ABC DLBCL subgroup characterized by upregulated MYC. Consistent with this notion, a high-MYC expressing human Burkitt lymphoma cell line was more sensitive to nucleotide biosynthesis inhibition than a low-MYC expressing cell line (*Online Supplementary Figure S7*).

Akin to *Atm*$^{-/-}$*nu*$^{-/-}$ lymphoma cells, cytotoxicity of these nucleotide biosynthesis inhibitors was exerted via apoptosis in high MYC-expressing human DLBCL (OC-ILY3) (Figure 8A, B), likely due to exacerbation of replication stress as evidenced by retention of cells in quiescent S-phase and activation of the replication stress response (Figure 8C-E). Taken together, these results show that response to nucleotide depletion in human lymphoma is influenced by MYC expression rather than *ATM* mutation status, thus demonstrating its broad applicability as a therapeutic approach independent of the mechanism underlying MYC dysregulation. Also, whilst the *Atm*$^{-/-}$*nu*$^{-/-}$ lymphomas and derived cell lines provide a model for DLBCL developed by A-T patients this could potentially also be useful for patients with high MYC-expressing DLBCL without A-T.

Discussion

High-grade B-NHL is the commonest tumor type in patients with A-T, representing 37-53% of cancer diagnoses in these individuals.[14,15] However, only a proportion of A-T patients develop tumors,[14] and the mechanisms of B-cell tumorigenesis underlying *ATM* loss remains unresolved. Moreover, the use of chemoradiotherapy for lymphoma treatment can be especially toxic for these patients owing to their inherent cellular chemoradiosensitivity.[14] Hence, the identification of therapeutic targets and development of alternative cancer treatments represents a critical unmet need.

In this context, our *Atm*$^{-/-}$*nu*$^{-/-}$ murine model closely recapitulates conditions under which lymphomagenesis occurs in human A-T including thymic aplasia and retention of a low-level of T cells arrested at the $CD3^{+}CD8^{+}$ and $CD3^{+}CD4^{+}$ differentiation stage.[22] Importantly, *Atm*$^{-/-}$*nu*$^{-/-}$ mice retained germinal centers and developed GCB as well as ABC DLBCL,

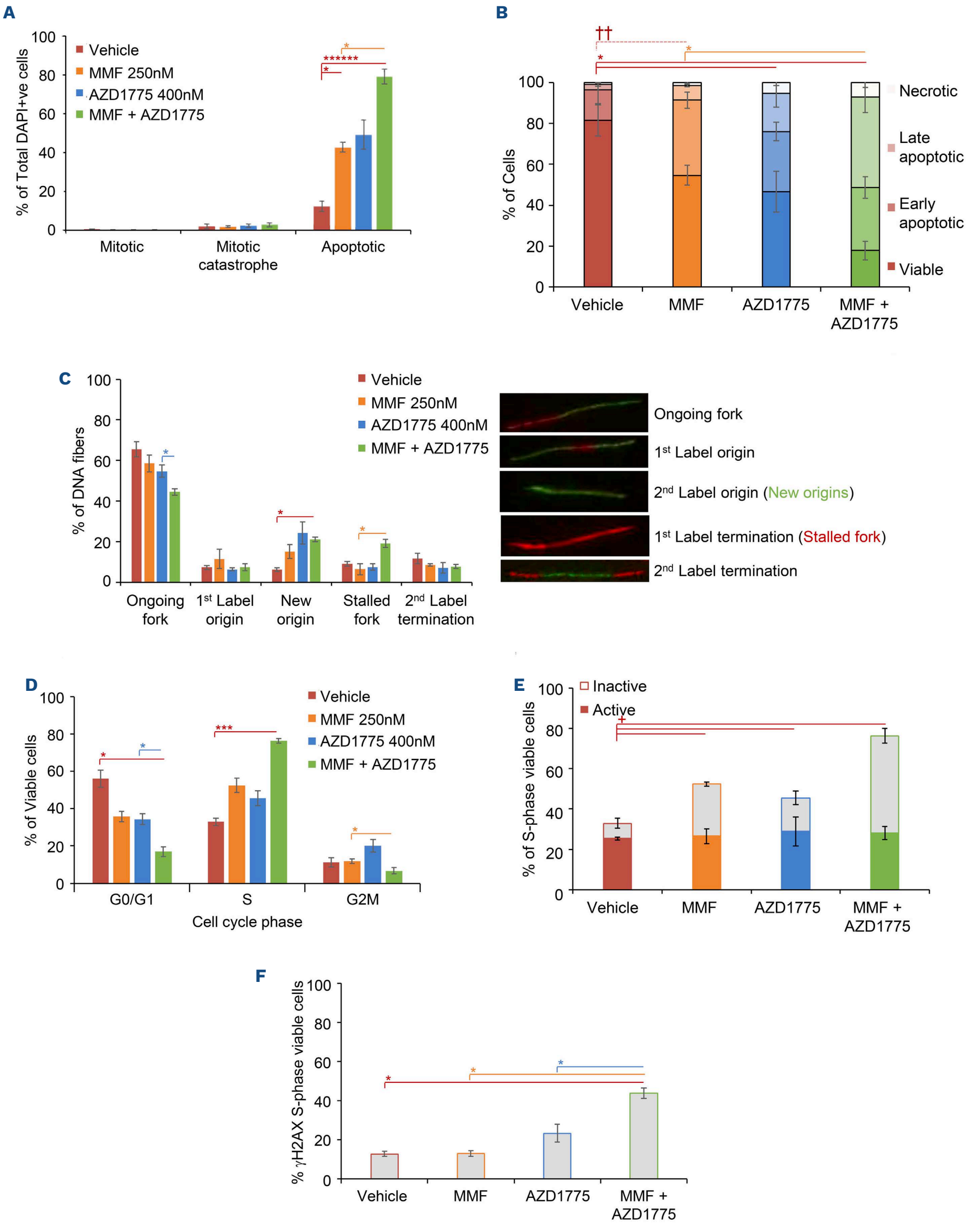

Continued on following page.

Figure 6. Nucleotide depletion induces replication stress-mediated apoptosis in *Atm*$^{-/-}$*nu*$^{-/-}$ lymphomas. (A, B) Exposure (72 hours [h]) of *Atm*$^{-/-}$*nu*$^{-/-}$ lymphoma cell lines (703, 5F3, 50F2) to vehicle, mycophenolate mofetil (MMF) (250 nM) or adavosertib (AZD1775) (400 nM), alone or in combination, led to cell death primarily via apoptosis. (A) Apoptosis was distinguished from mitotic catastrophe by 4',6-diamidino-2-phenylindole (DAPI)$^{+}$/lamin B^{-}/phospho (p)-histone H3-S10-immunofluorescence staining in the former, and DAPI^{+}/lamin B^{+}/p-histone H3-S10– staining in the latter. (B) Apoptosis was confirmed by annexin V (AxV)/propidium iodide status (PI): viable (AxV^{-}/PI^{-}), early apoptotic (AxV^{+}/PI^{-}), late apoptotic (AxV^{+}/PI^{+}), secondary necrotic (AxV^{-}/PI^{+}). (C) Replication fork progression in *Atm*$^{-/-}$*nu*$^{-/-}$ lymphomas measured by DNA fiber analysis; was significantly impeded by combination treatment with AZD1775 and MMF. (D) Cell cycle profiles of an *Atm*$^{-/-}$*nu*$^{-/-}$ lymphoma (50F2, N=3) showed an accumulation of tumor cells in S-phase upon combination treatment with AZD1775 and MMF. (E) Replicating (active, EDU^{+}) and non-replicating (inactive, EDU^{-}) cells in S-phase were distinguished by EDU positivity. In an *Atm*$^{-/-}$*nu*$^{-/-}$ lymphoma (50F2, N=3), combined treatment with AZD1775 and MMF led to accumulation of non-replicating cells residing in S-phase. (F) The proportion of γH2AX^{+} cells in non-replicating (inactive, EDU^{-}) S-phase was determined by flow cytometry. Combined treatment with AZD1775 and MMF resulted in γH2AX accumulation in *Atm*$^{-/-}$*nu*$^{-/-}$ lymphoma cells (50F2, N=3). Data are presented as mean ± standard error of the mean of (A-C) the 3 cell lines (703, 5F3, 50F2) or (D-F) 50F2. All experiments were performed at least in triplicate. Statistical significance ascertained by (A-E) matched multi-comparison two-way ANOVA with Tukey *post hoc* test and (F) repeat-measures matched multi-comparison one-way ANOVA with Tukey *post hoc* test denoted by: $^{*}P\leq0.05$, $^{**}P\leq0.01$, $^{***}P\leq0.005$, $^{****}P\leq0.001$, $^{*****}P\leq0.0005$, $^{******}P\leq0.0001$. (B) Statistical significance of viable (*), early apoptotic (†), late apoptotic (+), or necrotic (‡) cells. (E) Inactive cell comparison (+).

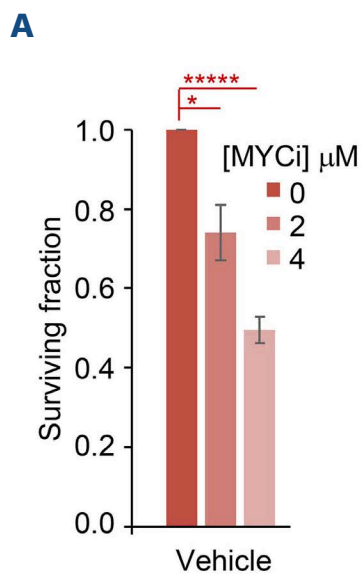

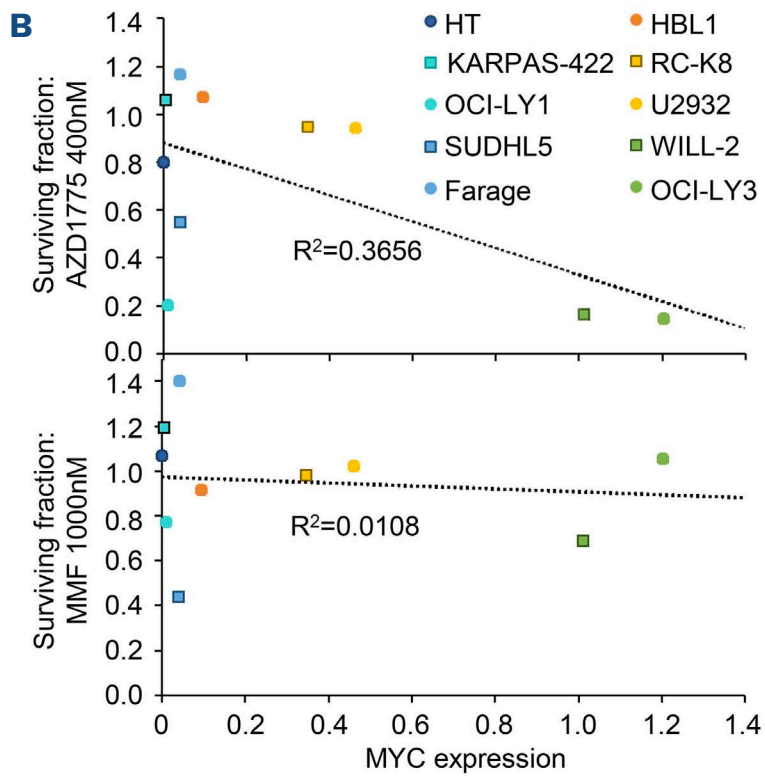

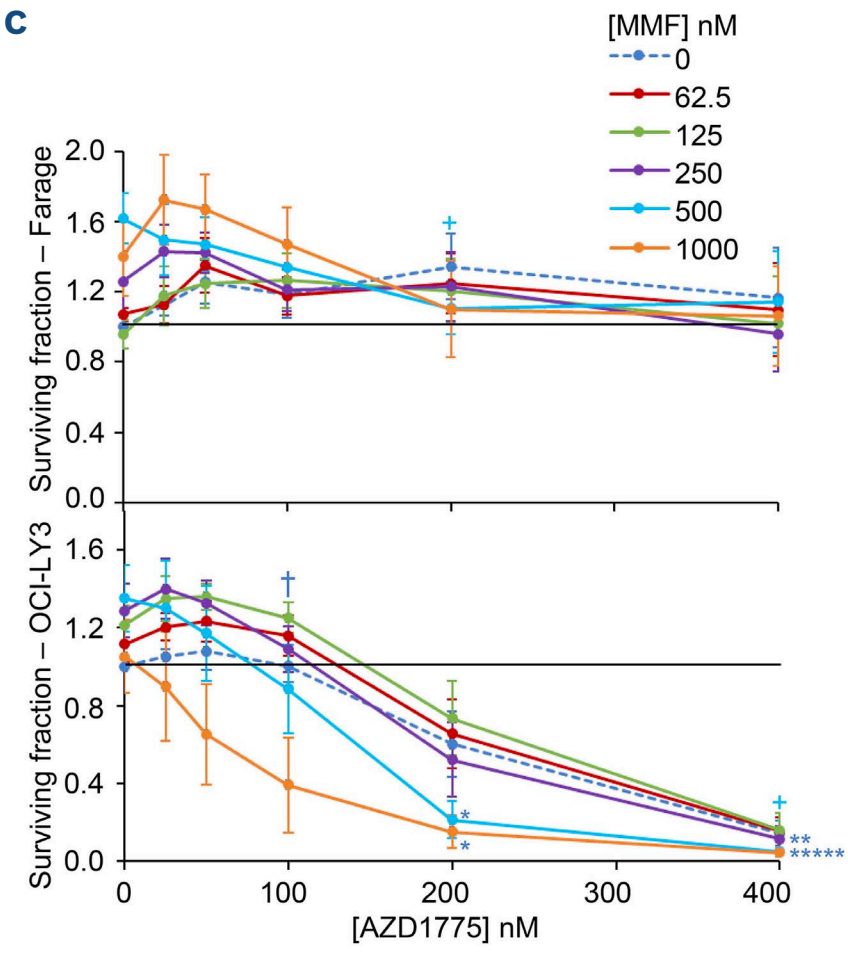

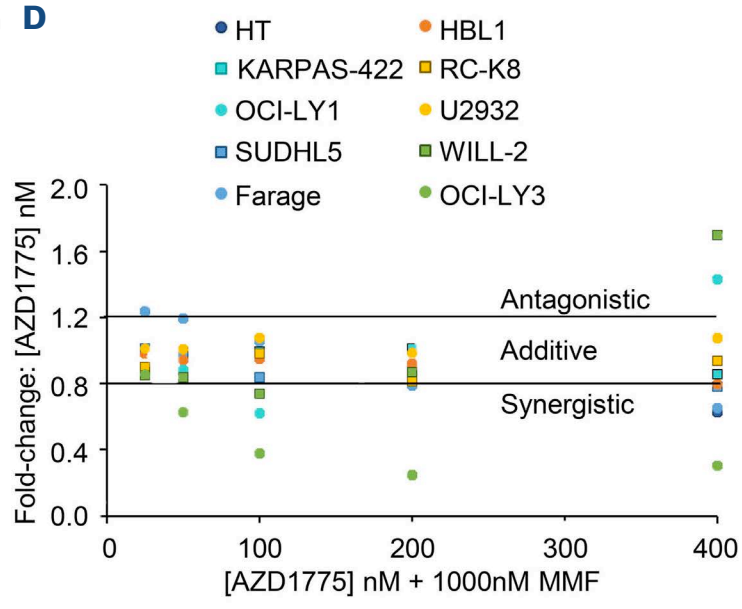

Continued on following page.

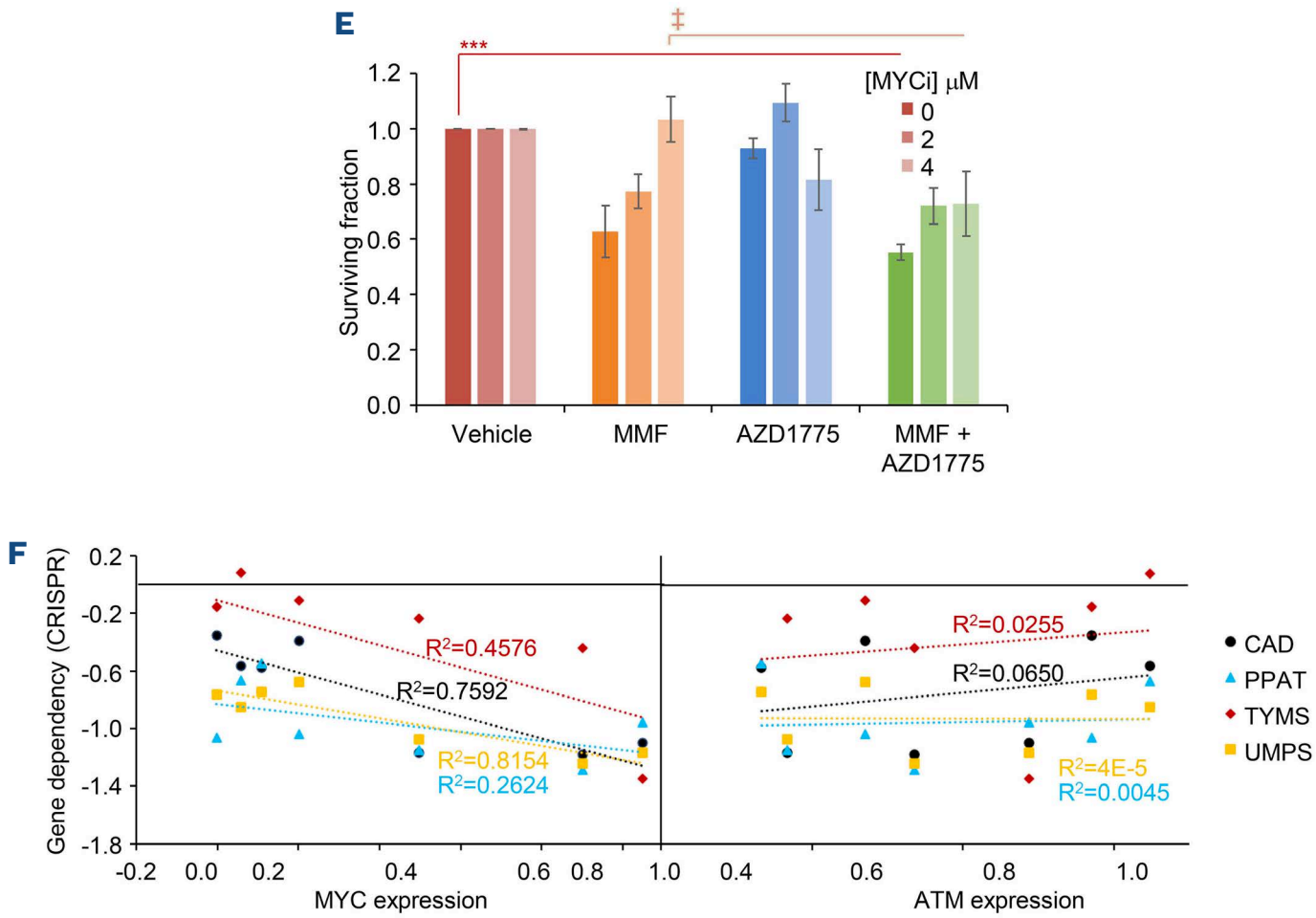

Figure 7. High MYC expression sensitizes human diffuse large B-cell lymphoma cells to AZD1775-induced nucleotide depletion. (A) Exposure of OCI-LY3, the human diffuse large B-cell lymphoma (DLBCL) cell line with high MYC expression to the MYC inhibitor (MYCi, MYCi361); at doses reported (Selleckchem) to specifically inhibit MYC activity; for 72 hours (h), led to significant toxicity as measured by CellTitre-Glo assay (N=5). (B) Exposure of 11 human DLBCL cell lines with varying MYC protein expression; determined by western blot with band intensities quantified using Image J normalized to vinculin; to physiologically attainable concentrations of mycophenolate mofetil (MMF) or adavosertib (AZD1775) indicated a correlation between MYC expression (low, blue; intermediate, orange; high, green) and increased AZD1775 cytotoxicity as measured by the CellTitre-Glo assay. (C) Dose response curves in 2 representative DLBCL cell lines show significant cytotoxicity with combined MMF and AZD1775 treatment in high MYC-expressing OCI-LY3 but not low MYC-expressing Farage. (D) Fold change representing the ratio of the surviving fraction following exposure to various AZD1775 + MMF dose combinations *versus* AZD1775 alone for the 11 human DLBCL cell lines. A fold change <0.8 indicates synergism and >1.2 indicates antagonism. Cell lines expressing high levels of MYC (green) are synergistically sensitive to the combined treatment. (E) Treatment of the OCI-LY3 cell line with a MYC inhibitor (MYCi, MYCi361) reduced its sensitivity to single-agent MMF (1,000 nM) and combined treatment with MMF (1,000 nM) and AZD1775 (200 nM) (N=5). Surviving fraction was normalized to the appropriate MYCi dose to highlight any rescue from MMF and/or AZD1775 toxicity. (F) Data-mining of the DepMap database reveals that protein expression of the top hits identified in the CRISPR/Cas9-mediated loss-of-function screen inversely correlate with MYC but not ATM expression in human DLBCL. (A, C, E) Cytotoxicity experiments were conducted on ≥5 separate occasions and data presented as mean ± standard error of the mean (SEM). Statistical significance *versus* vehicle (*), MMF (†), AZD1775 (+), or MMF + MYCi (‡), was ascertained by matched multi-comparison (A) one-way or (C, E) two-way ANOVA with Tukey *post hoc* test denoted by: $^{*}P\leq0.05$, $^{**}P\leq0.01$, $^{***}P\leq0.005$, $^{****}P\leq0.001$, $^{*****}P\leq0.0005$.

reminiscent of the phenotypic spectrum in ATM-defective human DLBCL.[9] In order to enable unbiased discovery of additional pathogenic processes and targetable lymphoma addictions, we systematically interrogated our *Atm*$^{-/-}$*nu*$^{-/-}$ model with genome-scale technology incorporating RNA-seq and CRISPR/Cas9 loss-of-function screens, approaches that have not previously been utilized to study ATM-defective DLBCL.

Our analysis uncovered a MYC-driven lymphoproliferation occurring in the context of constitutional *ATM* loss that characterizes A-T. However, whilst ATM inactivation initiates the genesis of *Atm*$^{-/-}$*nu*$^{-/-}$ lymphomas, it remains unclear whether ATM deficiency is an ongoing dependency in these tumors. Furthermore, well-known genetic mechanisms involving chromosomal rearrangements or gene amplifications only give rise to ~35% of MYC overexpressing high-grade B-NHL.[3-5,25] Likewise, genetic disruptions involving *Myc* were observed in some *Atm*$^{-/-}$*nu*$^{-/-}$ lymphomas but were absent in other instances of MYC dysregulation. Thus, future studies are required to determine the long-term effect of ATM deficiency on lymphomagenesis and the mechanisms that contribute to MYC activation in this murine model.

Our analysis revealed actionable dependencies beyond B-cell receptor signaling in *ATM*-defective DLBCL. In fact, from our CRISPR/Cas9 screens we observed dependency on key B-cell receptor signaling genes in only one of two evaluated *Atm*$^{-/-}$*nu*$^{-/-}$ lymphoma cell lines (50F2). On the contrary, nucleotide biosynthesis emerged as one of

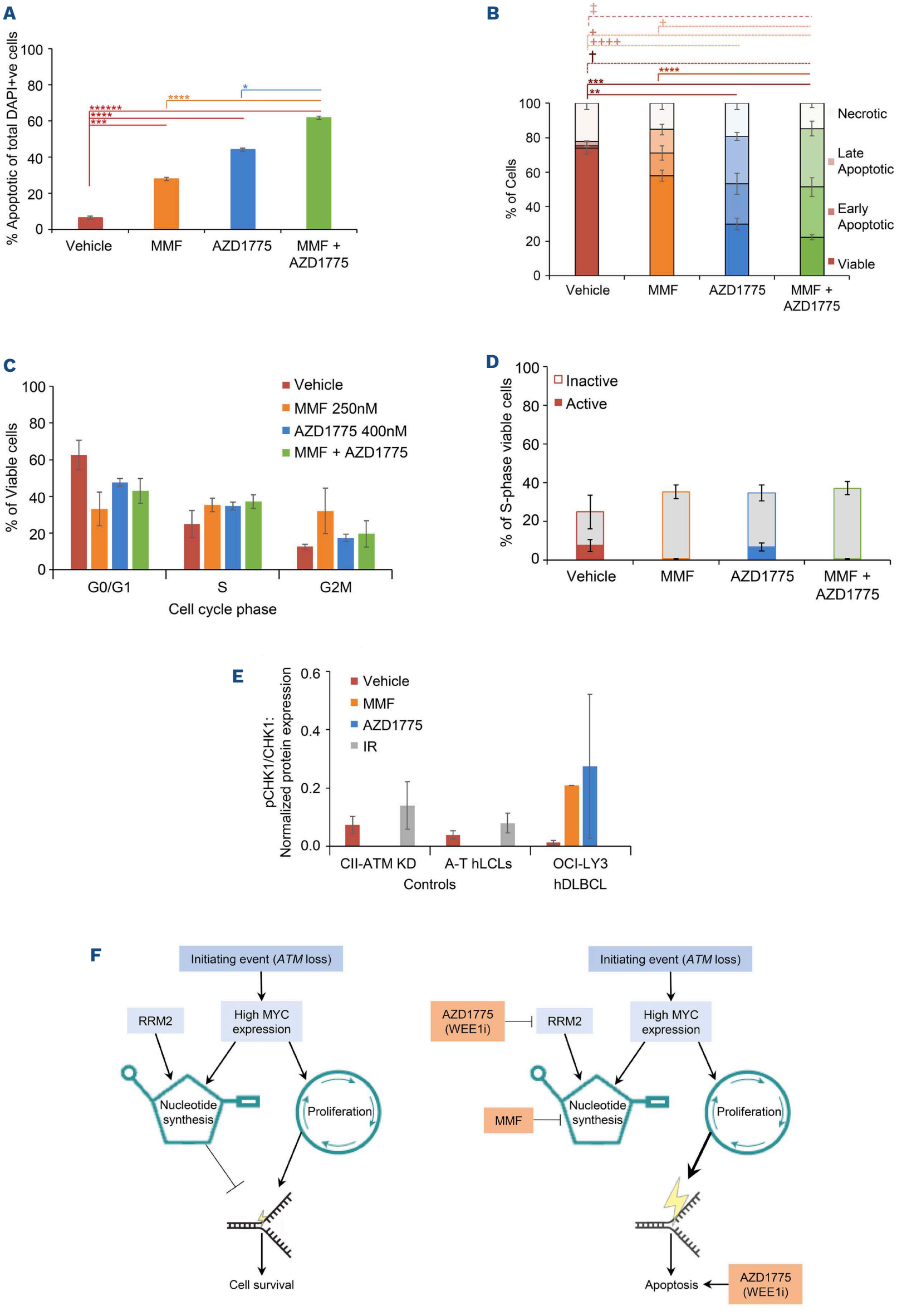

Continued on following page.

Figure 8. Nucleotide depletion induces replication stress-mediated apoptosis in human diffuse large B-cell lymphoma cells with high MYC expression. (A-E) Exposure (72 hours [h]) of OCI-LY3; a representative human diffuse large B-cell lymphoma (DLBCL) cell line with high MYC expression; to vehicle, mycophenolate mofetil (MMF) (1,000 nM) or adavosertib 1775 (AZD1775) (200 nM), alone or in combination, led to (A, B) cell death primarily via apoptosis as ascertained by (A) DAPI staining (N=4) and confirmed by (B) annexin V/propidium iodide (AxV/PI) status (N=4): viable (AxV^-/PI^-), early apoptotic (AxV^+/PI^-), late apoptotic (AxV^+/PI^+), and secondary necrotic (AxV^-/PI^+). (C) Cell cycle profiles showed an accumulation of cells in S-phase upon all treatments (N=4). (D) MMF (1,000 nM) treatment alone and in combination with AZD1775 (200 nM) led to accumulation of non-replicating (inactive, EDU^-) cells residing in S-phase (N=4). (E) Replication stress response generated by either AZD1775 or MMF treatment is evident in the high MYC-expressing OCI-LY3 DLBCL cell line. Irradiated (IR, 6 Gy, 30 minutes) CII-ATM KD CLL cell line and A-T patient-derived lymphoma cell lines (LCL) serve as positive controls. Band intensities quantified using Image J were normalized to vinculin from ≥3 western blots. (F) Schematic summarizing the mechanistic basis of targeting nucleotide biosynthesis in MYC-overexpressing DLBCL. (A-E) Experiments were conducted on ≥3 separate occasions and data presented as mean ± standard error of the mean. Statistical significance *versus* vehicle (red), MMF (orange), AZD1775 (blue), viable (*), early apoptotic (†), late apoptotic or inactive (+), or necrotic (‡), was ascertained by matched multi-comparison (A) one-way or (B-D) two-way ANOVA with Tukey *post hoc* test denoted by: $^{*}P\leq0.05$, $^{**}P\leq0.01$, $^{***}P\leq0.005$, $^{****}P\leq0.001$, $^{*****}P\leq0.0005$, $^{******}P\leq0.0001$.

the most prominent dependencies in both lymphoma lines, alongside DNA repair, DNA replication and cell cycle regulation, which were also significantly upregulated processes in our RNA-seq dataset. We showed that nucleotide metabolism in the context of *Atm* loss is a MYC-dependent vulnerability, which can be effectively targeted by nucleotide depletion through the synergistic actions of MMF and AZD1775. Our findings are consistent with a mechanistic model in which MYC induces replication stress by multiple transcription-dependent[44] and transcription-independent mechanisms.[31,45] Moderate levels of replication stress support tumor progression via generation of genomic instability whilst excessive levels are prevented by MYC-regulated nucleotide biosynthesis that becomes essential for tumor survival.[46] Combining MMF and AZD1775 potently inhibits nucleotide biosynthesis, leading to depletion of cellular dNTP that exacerbates replication stress. In turn, the accumulation of replication stress to catastrophic levels results in lymphoma lethality (Figure 8F). It remains to be determined whether other causes of replication stress or different mechanisms can render lymphoma cells dependent on nucleotide biosynthesis in the absence of MYC upregulation, as observed in two DLBCL cell lines with low MYC expression.

Targeted therapies, such as ibrutinib, have been associated with disappointing responses[47] coupled with possible enrichment of cells overexpressing MYC targets in ibrutinib-resistant DLBCL.[48] We confirmed the broad applicability of nucleotide depletion as a therapeutic strategy for MYC-driven DLBCL independent of *ATM* status in human DLBCL models. In this regard, a previous study showed that inhibition of phosphoribosyl pyrophosphate synthetase 2, an enzyme essential for purine biosynthesis, is synthetically lethal in MYC-driven murine lymphoma.[49] Herein, we demonstrated a complementary strategy to inhibit nucleotide biosynthesis in DLBCL through synthetic lethality between RRM2 depletion and MYC overexpression, which is potentiated in the presence of MMF (Figure 8F). We showed that depletion of RRM2, a ribonucleotide reductase subunit essential for nucleotide biosynthesis, can be achieved through AZD1775, the WEE1 inhibitor under active clinical investigation in DLBCL (*clinicaltrials gov. Identifier: NCT02465060, NCT04439227*). Indeed, a recent study demonstrating selectivity of AZD1775 monotherapy against MYC-overexpressing DLBCL[41] lends further support to a synthetically lethal interaction between MYC overexpression and RRM2 loss. While clinical trials in solid tumors showed AZD1775 to be generally well-tolerated,[50-52] our findings support the clinical evaluation of the AZD1775-MMF combination in DLBCL, including among A-T patients. Our results also support the investigation of MYC overexpression as a predictive biomarker of response to inform patient selection into these trials.

Finally, our CRISPR/Cas9 screen identified other core components within the purine or pyrimidine biosynthetic pathway that could serve as synthetically lethal partners with MYC overexpression and/or *ATM* loss, and therefore deserve further investigation as therapeutic targets. These include phosphoribosyl pyrophosphate amidotransferase (PPAT), carbamoyl-phosphate synthetase (CAD), thymidylate synthetase (TYMS) and uridine 5'-monophosphate synthase (UMPS). Collectively, our findings highlight nucleotide metabolism as a compelling therapeutic vulnerability with potential for further development into a novel treatment paradigm for clinically high-risk, MYC-driven lymphoma. This approach is garnering interest in hemato-oncology with a dihydroorotate dehydrogenase inhibitor (BAY2402234) already in a phase I clinical trial for myeloid malignancies.[53,54]

Disclosures

MO'C and JVF are full-time employees and shareholders

at AstraZeneca. The other authors have no conflicts of interest to disclose.

Contributions

ND, TF, CO, MA, JW. PJB, MB, MH, RZ, MI, TP, AA, A-MH, ES, GK and CC performed experiments. ND, TF, CO, AS-O, PK, SA, MH, CB, PGM, EF and MK analyzed results. ND, TF, PJB, MO'C, JVF, GSS, TS and AMT designed the research. ND, TF, CO, TS, MK and AMT wrote the paper.

Acknowledgments

We thank Mike Griffiths (West Midlands Regional Genetics Laboratory) and Robert Hollows (Institute of Cancer and Genomic Sciences) for their expertise with data analysis; Paloma Garcia (Institute of Cancer and Genomic Sciences), Rachel Bayley (Institute of Cancer and Genomic Sciences) and Clare Shannon-Lowe (Institute of Immunology and Immunotherapy) for experimental assistance; and the University of Birmingham Genomics Sequencing and Flow Cytometry Services for analytical help.

Funding

This work was supported by grants from CRUK (ref: C20807/A2864 and C17183/A23303), Bloodwise UK (program grant 11045) and Action for A-T (Ref: 17-1192). CB was supported by grants from MRC and BCUK. PM was also supported in part by a European Regional Development Fund Project (ENOCH: CZ.02.1.01/0.0/0.0/16_019/0000868). MK is a Cancer Research UK Clinicial Scientist.

Data-sharing statement

RNA-seq and CRISPR data are available at GEO: https://www.ncbi.nlm.nih.gov/geo/query/acc.cgi?acc=GSE215877.

References

1. Ott G, Rosenwald A, Campo E. Understanding MYC-driven aggressive B-cell lymphomas: pathogenesis and classification. Blood. 2013;122(24):3884-3891.
2. Sehn LH, Salles G. Diffuse large B-cell lymphoma. N Engl J Med. 2021;384(9):842-858.
3. Copie-Bergman C, Cuilliere-Dartigues P, Baia M, et al. MYC-IG rearrangements are negative predictors of survival in DLBCL patients treated with immunochemotherapy: a GELA/LYSA study. Blood. 2015;126(22):2466-2474.
4. Horn H, Ziepert M, Becher C, et al. MYC status in concert with BCL2 and BCL6 expression predicts outcome in diffuse large B-cell lymphoma. Blood. 2013;121(12):2253-2263.
5. Staiger AM, Ziepert M, Horn H, et al. Clinical impact of the cell-of-origin classification and the MYC/ BCL2 dual expresser status in diffuse large B-cell lymphoma treated within prospective clinical trials of the German High-Grade Non-Hodgkin's Lymphoma Study Group. J Clin Oncol. 2017;35(22):2515-2526.
6. Scott DW, King RL, Staiger AM, et al. High-grade B-cell lymphoma with MYC and BCL2 and/or BCL6 rearrangements with diffuse large B-cell lymphoma morphology. Blood. 2018;131(18):2060-2064.
7. Rosenwald A, Bens S, Advani R, et al. Prognostic significance of MYC rearrangement and translocation partner in diffuse large B-cell lymphoma: a study by the Lunenburg Lymphoma Biomarker Consortium. J Clin Oncol. 2019;37(35):3359-3368.
8. Petrich AM, Gandhi M, Jovanovic B, et al. Impact of induction regimen and stem cell transplantation on outcomes in double-hit lymphoma: a multicenter retrospective analysis. Blood. 2014;124(15):2354-2361.
9. Reddy A, Zhang J, Davis NS, et al. Genetic and functional drivers of diffuse large B cell lymphoma. Cell. 2017;171(2):481-494.e15.
10. Melchardt T, Hufnagl C, Weinstock DM, et al. Clonal evolution in relapsed and refractory diffuse large B-cell lymphoma is characterized by high dynamics of subclones. Oncotarget. 2016;7(32):51494-51502.
11. Leeksma OC, de Miranda NF, Veelken H. Germline mutations predisposing to diffuse large B-cell lymphoma. Blood Cancer J. 2017;7(2):e532.
12. Grønbaek K, Worm J, Ralfkiaer E, Ahrenkiel V, Hokland P, Guldberg P. ATM mutations are associated with inactivation of the ARF-TP53 tumor suppressor pathway in diffuse large B-cell lymphoma. Blood. 2002;100(4):1430-1437.
13. Xu-Monette ZY, Zhang H, Zhu F, et al. A refined cell-of-origin classifier with targeted NGS and artificial intelligence shows robust predictive value in DLBCL. Blood Adv. 2020;4(14):3391-3404.
14. Suarez F, Mahlaoui N, Canioni D, et al. Incidence, presentation, and prognosis of malignancies in ataxia-telangiectasia: a report from the French national registry of primary immune deficiencies. J Clin Oncol. 2015;33(2):202-208.
15. Bakhtiar S, Salzmann-Manrique E, Donath H, et al. The incidence and type of cancer in patients with ataxia-telangiectasia via a retrospective single-centre study. Br J Haematol. 2021;194(5):879-887.
16. Rothblum-Oviatt C, Wright J, Lefton-Greif MA, McGrath-Morrow SA, Crawford TO, Lederman HM. Ataxia telangiectasia: a review. Orphanet J Rare Dis. 2016;11(1):159.
17. Lee JH, Paull TT. Cellular functions of the protein kinase ATM and their relevance to human disease. Nat Rev Mol Cell Biol. 2021;22(12):796-814.
18. Hathcock KS, Padilla-Nash HM, Camps J, et al. ATM deficiency promotes development of murine B-cell lymphomas that resemble diffuse large B-cell lymphoma in humans. Blood. 2015;126(20):2291-2301.
19. Li W, Xu H, Xiao T, et al. MAGeCK enables robust identification of essential genes from genome-scale CRISPR/Cas9 knockout screens. Genome Biol. 2014;15(12):554.
20. Barlow C, Hirotsune S, Paylor R, et al. Atm-deficient mice: a paradigm of ataxia telangiectasia. Cell. 1996;86(1):159-171.
21. Xu Y, Ashley T, Brainerd EE, Bronson RT, Meyn MS, Baltimore D. Targeted disruption of ATM leads to growth retardation, chromosomal fragmentation during meiosis, immune defects, and thymic lymphoma. Genes Dev. 1996;10(19):2411-2422.
22. Chopra C, Davies G, Taylor M, et al. Immune deficiency in Ataxia-Telangiectasia: a longitudinal study of 44 patients. Clin Exp Immunol. 2014;176(2):275-282.

23. Alizadeh AA, Eisen MB, Davis RE, et al. Distinct types of diffuse large B-cell lymphoma identified by gene expression profiling. Nature. 2000;403(6769):503-511.
24. Wright G, Tan B, Rosenwald A, Hurt EH, Wiestner A, Staudt LM. A gene expression-based method to diagnose clinically distinct subgroups of diffuse large B cell lymphoma. Proc Natl Acad Sci U S A. 2003;100(17):9991-9996.
25. Pophali PA, Marinelli LM, Ketterling RP, et al. High level MYC amplification in B-cell lymphomas: is it a marker of aggressive disease? Blood Cancer J. 2020;10(1):5.
26. Liyanage M, Weaver Z, Barlow C, et al. Abnormal rearrangement within the alpha/delta T-cell receptor locus in lymphomas from Atm-deficient mice. Blood. 2000;96(5):1940-1946.
27. Maclean KH, Kastan MB, Cleveland JL. Atm deficiency affects both apoptosis and proliferation to augment Myc-induced lymphomagenesis. Mol Cancer Res. 2007;5(7):705-711.
28. Shreeram S, Hee WK, Demidov ON, et al. Regulation of ATM/p53-dependent suppression of myc-induced lymphomas by Wip1 phosphatase. J Exp Med. 2006;203(13):2793-2799.
29. Pusapati RV, Rounbehler RJ, Hong S, et al. ATM promotes apoptosis and suppresses tumorigenesis in response to Myc. Proc Natl Acad Sci U S A. 2006;103(5):1446-1451.
30. Curti L, Campaner S. MYC-induced replicative stress: a double-edged sword for cancer development and treatment. Int J Mol Sci. 2021;22(12):6168.
31. Dominguez-Sola D, Ying CY, Grandori C, et al. Non-transcriptional control of DNA replication by c-Myc. Nature. 2007;448(7152):445-451.
32. Bester AC, Roniger M, Oren YS, et al. Nucleotide deficiency promotes genomic instability in early stages of cancer development. Cell. 2011;145(3):435-446.
33. Hastak K, Paul RK, Agarwal MK, et al. DNA synthesis from unbalanced nucleotide pools causes limited DNA damage that triggers ATR-CHK1-dependent p53 activation. Proc Natl Acad Sci U S A. 2008;105(17):6314-6319.
34. Poli J, Tsaponina O, Crabbe L, et al. dNTP pools determine fork progression and origin usage under replication stress. EMBO J. 2012;31(4):883-894.
35. Zeman MK, Cimprich KA. Causes and consequences of replication stress. Nat Cell Biol. 2014;16(1):2-9.
36. Allison AC, Eugui EM. Mycophenolate mofetil and its mechanisms of action. Immunopharmacology. 2000;47(2-3):85-118.
37. Pfister SX, Markkanen E, Jiang Y, et al. Inhibiting WEE1 selectively kills histone H3K36me3-deficient cancers by dNTP starvation. Cancer Cell. 2015;28(5):557-568.
38. Adams JM, Harris AW, Pinkert CA, et al. The c-myc oncogene driven by immunoglobulin enhancers induces lymphoid malignancy in transgenic mice. Nature. 1985;318(6046):533-538.
39. Ge XQ, Jackson DA, Blow JJ. Dormant origins licensed by excess Mcm2-7 are required for human cells to survive replicative stress. Genes Dev. 2007;21(24):3331-3341.
40. Ibarra A, Schwob E, Mendez J. Excess MCM proteins protect human cells from replicative stress by licensing backup origins of replication. Proc Natl Acad Sci U S A. 2008;105(26):8956-8961.
41. Young LA, O'Connor LO, de Renty C, et al. Differential activity of ATR and WEE1 inhibitors in a highly sensitive subpopulation of DLBCL linked to replication stress. Cancer Res. 2019;79(14):3762-3775.
42. Schmitz R, Wright GW, Huang DW, et al. Genetics and pathogenesis of diffuse large B-cell lymphoma. N Engl J Med. 2018;378(15):1396-1407.
43. Tsherniak A, Vazquez F, Montgomery PG, et al. Defining a cancer dependency map. Cell. 2017;170(3):564-576.e516.
44. Lin CY, Loven J, Rahl PB, et al. Transcriptional amplification in tumor cells with elevated c-Myc. Cell. 2012;151(1):56-67.
45. Macheret M, Halazonetis TD. Intragenic origins due to short G1 phases underlie oncogene-induced DNA replication stress. Nature. 2018;555(7694):112-116.
46. Liu YC, Li F, Handler J, et al. Global regulation of nucleotide biosynthetic genes by c-Myc. PLoS One. 2008;3(7):e2722.
47. Wilson WH, Young RM, Schmitz R, et al. Targeting B cell receptor signaling with ibrutinib in diffuse large B cell lymphoma. Nat Med. 2015;21(8):922-926.
48. Shaffer AL, 3rd, Phelan JD, Wang JQ, et al. Overcoming acquired epigenetic resistance to BTK inhibitors. Blood Cancer Discov. 2021;2(6):630-647.
49. Cunningham JT, Moreno MV, Lodi A, Ronen SM, Ruggero D. Protein and nucleotide biosynthesis are coupled by a single rate-limiting enzyme, PRPS2, to drive cancer. Cell. 2014;157(5):1088-1103.
50. Do K, Wilsker D, Ji J, et al. Phase I study of single-agent AZD1775 (MK-1775), a Wee1 kinase inhibitor, in patients with refractory solid tumors. J Clin Oncol. 2015;33(30):3409-3415.
51. Liu JF, Xiong N, Campos SM, et al. Phase II study of the WEE1 inhibitor adavosertib in recurrent uterine serous carcinoma. J Clin Oncol. 2021;39(14):1531-1539.
52. Seligmann JF, Fisher DJ, Brown LC, et al. Inhibition of WEE1 is effective in TP53- and RAS-mutant metastatic colorectal cancer: a randomized trial (FOCUS4-C) comparing adavosertib (AZD1775) with active monitoring. J Clin Oncol. 2021;39(33):3705-3715.
53. Christian S, Merz C, Evans L, et al. The novel dihydroorotate dehydrogenase (DHODH) inhibitor BAY 2402234 triggers differentiation and is effective in the treatment of myeloid malignancies. Leukemia. 2019;33(10):2403-2415.
54. Sexauer AN, Alexe G, Gustafsson K, et al. DHODH: a promising target in the treatment of T-Acute Lymphoblastic Leukemia. Blood Adv. 2023;7(21):6685-6701.
55. Morin RD, Johnson NA, Severson TM, et al. Somatic mutations altering EZH2 (Tyr641) in follicular and diffuse large B-cell lymphomas of germinal-center origin. Nat Genet. 2010;42(2):181-185.
56. Beguelin W, Popovic R, Teater M, et al. EZH2 is required for germinal center formation and somatic EZH2 mutations promote lymphoid transformation. Cancer Cell. 2013;23(5):677-692.
57. Liberzon A, Birger C, Thorvaldsdottir H, Ghandi M, Mesirov JP, Tamayo P. The molecular signatures database (MSigDB) hallmark gene set collection. Cell Syst. 2015;1(6):417-425.